

We would like to thank the anonymous reviewer#1 for the comments and suggestions, which have helped improve the clarity and readability of this paper notably.

ANSWERS TO REVIEWER# 1

General comments:

1. Some modifications and an english checking have been made. See changes.
2. General rules have been applied. See changes in all the document.
3. Some captions have been changed in order to better describe the figures.
4. The abstract has been rewritten in order to describe main results and also the bias correction issues have been included.
5. The introduction has been shortened and rearranged as suggested by the reviewer according to the specific comments.

Specific comments:

1.: Correction made

2.: The abstract has completely changed, see changes.

3-10: Modifications have been made.

11-12: Following recommendations of 2 reviewers, the introduction has been changed and shortened.

13-15: Modifications have been made

16: This paragraph has been shortened.

17: This sentence has been removed.

18-21: Modifications have been made

22: The sentence has been changes by: "The signal to noise ratio is still not high today, thus retrievals algorithms must be improved."

23-30: Suggestions were taken into account.

31: The sentences have been modified. Due to large known biases in precipitation, a satellite-based large-scale correction of precipitation is applied to the precipitation fluxes. This correction has been inferred from the comparison between the Remote Sensing Systems (RSS) Passive Microwave

Water Cycle (PMWC) product (Hilburn, 2009) and the IFS ECMWF precipitation (Lellouche et al., 2013).

32-36: Suggestions were taken into account.

37: The term “progressively” has been changed by “incrementally “ that refers to the incremental Analyse Update (IAU).

38-39: Modifications have been made

40: A sentence has been added to explain how the representativity error is inferred: “Representativity errors concerning in situ observations were calculated a posteriori from a reanalysis over the period 2008-2012. The estimated errors are constant throughout the year. The method (Desroziers et al., 2005) consists of the computation of a ratio, which is a function of observation errors, innovations and residuals.”

41.: change made.

42.: Equations and text have been changed to clarify the purpose.

43.: change made.

44: No, it is correct. This term ξ refers to the satellite SSS bias we want to minimize which is different from x that refers to the salinity bias from surface in-situ data.

45-46: Done.

47.: We tried to clarify the 2 biases: The salinity in-situ bias at surface (x) and SSS (SMOS) bias (ξ) are different. The new figures 3 show the in-situ bias without the SSS (SMOS) bias (a), the SMOS SSS bias from space only (b) and the in-situ bias with the SSS SMOS bias.

48.: done

49: We have improved the explanation of the boot-strap method.

50.: As written, the a priori error R_{ξ}^o is a combination of a zonally varying error, together with an increase over regions with sparse in-situ data and near the coast. The algorithm to increase the error in case of sparse data and near the coast is not detailed in this paper.

51-60: Modifications have been made

61-62: This paragraph and Figures have changed.

63-65: Modifications have been made

66: The Matisse ship route location used for the comparison is shown. Figures and caption have been merged.

Data assimilation of SMOS observations into the Mercator Ocean operational system: focus on the Niño 2015 event

Benoît Tranchant¹, Elisabeth Remy², Eric Greiner¹ and Olivier Legalloudec²

¹Collecte Localisation Satellites, Ramonville Saint-Agne, 31520, France

5 ²Mercator-Océan, Ramonville Saint-Agne, 31520, France

Correspondence to: Benoît Tranchant (btranchant@groupcls.com)

Abstract. Monitoring Sea Surface Salinity (SSS) is important for understanding and forecasting the ocean circulation. It is even crucial in the context of the acceleration of the water cycle. Until recently, SSS was one of the less observed essential ocean variables. Only sparse in situ observations, mostly closer to 5 meters depth than the surface, were available to estimate the SSS. The recent satellite ESA Soil Moisture and Ocean Salinity ([SMOS](#)), NASA Aquarius SAC-D and Soil Moisture Active Passive ([SMAP](#)) missions have made possible for the first time to measure SSS from space.

The SSS drivers can be quite different than the temperature ones. The model SSS can suffer from significant errors coming not only from the ocean dynamical model but also the atmospheric precipitation and evaporation as well as ice melting and river runoff. Satellite SSS can bring a valuable additional constraint to control the model salinity.

15 This article presents the analysis of an Observing System Experiment (OSE) conducted with the $\frac{1}{4}^\circ$ resolution Mercator Ocean analysis and forecasting system. SSS data assimilation constrains the model SSS to be closer to the observations in a coherent way with the other data sets already routinely assimilated in an operational context. Globally, the SMOS SSS assimilation has a positive impact in salinity over the top 30 meters. Comparisons to independent data sets show a small but positive impact. The sea surface height (SSH) has also been impacted by implying a reinforcement of Tropical Instability Waves (TIWs) during the El-Niño 2015/16 event. Finally, this study helped us to progress in the understanding of the biases and errors that can degrade the SMOS SSS performance.

1 Introduction

Recent progress in data treatment of Sea Surface Salinity (SSS) from space make possible their assimilation in ocean analysis systems (Boutin et al., 2017). Since 2009 the launch of the European Space Agency (ESA) Soil Moisture and Ocean Salinity (SMOS) mission in 2009, then the launches of NASA's Aquarius in 2011 and Soil Moisture Active Passive (SMAP) in 2015, SSS are available and have been used in many studies (e.g., Tang et al., 2017, Vinogradova et al., 2014; Toyoda et al., 2015, Reul et al., 2013).

Here we present the impact of assimilating SSS observations from space into the global $\frac{1}{4}^\circ$ Mercator Ocean operational system (see Lellouche et al., 2013) evaluated in the SMOS Niño 2015 project (<https://www.godae-oceanview.org/projects/smos-Niño15>). The changes induced by assimilating the satellite SSS in addition to the observation data operationally assimilated

are analyzed. The focus has been primarily on the 2015-2016 El Niño event, in which strong SSS anomalies are seen in the Tropical Pacific in both model and observations (Hasson et al., 2018; Gasparin and Roemmich, 2016; Guimbard et al., 2017). The salinity plays an important role in the ocean-atmosphere coupling in this region by isolating the ocean interior due to the formation of a Barrier Layer. It is then not only the thermocline depth that is of importance but also the halocline when it becomes shallower than the thermocline.

The most striking event in the global ocean for the year 2015 was the strong El Niño event. It is as strong as the 1997 one, see section 2.6 in (Von Schuckmann et al., 2018). Several El Niño Southern Oscillation (ENSO) indices are used to monitor the tropical Pacific and based on Sea Surface Temperature (SST) anomalies averaged on different regions (e.g. NINO3.4 for the Nino3.4 region in the central Pacific, see Barnston et al., (1997)). Because the maximum of the SST anomalies stays off the eastern coast of South and Central America, it was more likely to be a Modoki El Niño (Ashok and Yamagata, 2009) or a central Pacific El Niño (Kao and Yu, 2009) than a classical eastern Pacific El Niño.

Warm anomalies began to build in the western pacific in 2014 triggered by Westerly Wind Bursts but did not lead to the development of an El Niño in the year. Moreover, as suggested by McPhaden et al., (2015), the presence of El Niño precursors in early-2014 helped the development of a strong El Niño at the end of 2015. Anomalous eastward currents along the equator and in the NECC continued a pattern from 2014. This is associated with an increase in precipitation and an eastward shift in fresh surface salinities. A strong equatorial SSS anomaly in 2015 has been observed and described, see for example (Hasson et al., 2018; Gasparin and Roemmich, 2016). The Pacific freshening is due to a strong ITCZ in 2015, but advection by anomalous eastward currents also plays a role in the SSS changes. The difference of the two annual anomalies in 2014 and 2015 in our control run (see section 3) is shown in Fig. 1. The 2015–2016 El Niño is also the first important climatic event fully captured by the SMOS satellite where negative SSS anomalies have been observed between 0 and 15°N around 170°W from mid-2014 to mid-2015 (Boutin et al., 2016).

Data assimilation experiments conducted within the SMOS Niño 2015 project (<https://www.godae-oceanview.org/projects/smos-Niño15>) are helping to prepare the assimilation of space SSS data and allow testing their impact on short term ocean forecast and analysis. To evaluate the impact of SSS observations from satellites on ocean monitoring and forecast systems in a realistic context, Observing System Experiments (OSEs) were conducted with the UK Met Office and Mercator Ocean global ocean forecast systems. The OSE approach is conducted by comparing two assimilation experiments which are identical except that the satellite SSS are withheld in the analysis in one of the experiments. The differences between the two simulations highlight the “impact” of the withheld observations. SST, SLA and in situ observations are assimilated as currently done in the operational systems, see Martin et al., (2018). Similar OSE approaches are generally used to evaluate observation networks in the ocean data assimilation community of GODAE OceanView (Oke et al., 2015, Lea et al., 2014). Experiments conducted within the SMOS Niño15 project to test the impact of the satellite SSS data were carefully designed and analyzed to ensure robust conclusions on the impact of SSS measurements on ocean analysis. The system used for the OSE is based on the operational ocean monitoring and forecasting system operated at Mercator Ocean. The use of such system ensures that conclusions are relevant for such operational applications.

To assess the benefit of assimilating SSS from satellite in a realistic context, all observations from the Global Ocean Observing System (GOOS) that are assimilated in real time ocean analysis or reanalysis are also assimilated. SST, in situ temperature and salinity observations (from moorings, drifting platforms, ships) and along track Sea Level Anomalies in the so-called Reference simulation are assimilated (hereafter REF). OSEs conducted were designed to assess the impact of weekly products as the system has a weekly assimilation cycle.

It is recommended to withhold part of the usually assimilated observations from the OSEs to have fully independent data to compare with, see Fuji et al., (2015). The TAO mooring salinity data were not assimilated and kept for verification. Even if restricted to the few mooring points, those data are the only ones to provide long term time series of daily temperature and salinity observations.

Several studies (Reul et al., 2013 or Lee et al., 2012) show that SSS measured from space can bring new information. Recently, (Toyoda et al., 2014; Hackert et al., 2014) show the impact of assimilating Aquarius data in the Pacific region both in uncoupled and coupled ocean-atmosphere systems. In a recent paper, Chakraborty et al., (2014) show that the migration of the thermohaline fronts at the eastern edge of the western Pacific warm pool can be more realistic with the assimilation of Aquarius SSS. Data assimilation of Aquarius SSS can also help to better understand the variability of salinity structure in the Bay of Bengal (Seelanki et al., 2018). Finally, SSS assimilation from space is promising in an operational context both for ocean and seasonal forecasting.

Nevertheless, technical challenges are still open to assimilate SSS data efficiently in the context of global ocean analysis and forecasting. The assimilation of satellite SSS observations is challenging because of the various complex biases, see Köhl et al, (2014). The difference between the forecast and the satellite SSS can be 5 times larger than the misfit between the forecast and near surface ARGO salinity. The signal to noise ratio is still not high today, thus retrievals algorithms must be improved. Careful analysis of the SSS data sets shows that a bias correction is needed before their assimilation as shown by Martin (2016). To have an optimal analysis, the hypothesis of un-biased errors has to be respected. This article details the bias correction scheme and the error estimation scheme used in the data assimilation system for those data. This is a necessary step to have a positive impact of SSS data assimilation.

The structure of this article is as follows: after a description of the OSE where the operational system, the bias correction, the SSS observation error and the presentation of the experimental design are described in section 2, the effect of the SMOS SSS data assimilation is discussed in section 3, while discussions and conclusions are provided in section 4.

2. OSE approach

The OSE are conducted with the global $\frac{1}{4}^\circ$ ocean analysis and forecasting system running in real time at Mercator Ocean. Detailed descriptions of the system can be found in (Lellouche et al., 2013; Lellouche et al., 2018). After a brief description of the system configuration, we will describe the data assimilation components that were specifically developed or adapted for the SSS data assimilation in detail.

2.1 Ocean model and configuration

The Mercator Ocean real time analysis and forecast is based on the version 3.1 of the NEMO ocean model (Madec, 2016), which uses a $\frac{1}{4}^\circ$ ORCA grid. The water column is discretized into 50 vertical levels, including 22 levels within the upper 100 m, with 1-m resolution at the surface to 450-m resolution at the bottom. The system has been initialized in autumn 2006, using temperature and salinity profiles from the EN4 climatology (Good et al., 2013).

The ocean model is forced by atmospheric fields from the European Centre for Medium-Range Weather Forecasts-Integrated Forecast System (ECMWF-IFS) at 3-hr resolution to reproduce the diurnal cycle. Momentum and heat turbulent surface fluxes are computed by using (Large and Yeager 2009) bulk formulae. Due to large known biases in precipitation, a satellite-based large-scale correction of precipitation is applied to the precipitation fluxes. This correction has been inferred from the comparison between the Remote Sensing Systems (RSS) Passive Microwave Water Cycle (PMWC) product (Hilburn, 2009) and the IFS ECMWF precipitation (Lellouche et al., 2013).

A monthly river runoff climatology is built with data on coastal runoff from 100 major rivers from the Dai et al. (2009) database instead of Dai and Trenberth (2002). This database uses new data, mostly from recent years, streamflow simulated by the Community Land Model version 3 (Verstentein et al., 2004) to fill the gaps, in all lands areas except Antarctica and Greenland.

At high latitudes the effect of iceberg melting is also parameterized. The lack of interannual variability of the largest rivers is known to lead to large errors in the surface ocean salinity in the analysis and forecast. There is no SSS relaxation term to any climatology like in the operational case. More details concerning parameterization of the terms included in the momentum, heat and freshwater balances (i.e, advection, diffusion, mixing and surface fluxes) can be found in (Lellouche et al., 2018).

2.2 Assimilated Observations

2.2.1 Regular observation data

All ocean observations assimilated in the real time forecasting system are assimilated in the same way in the OSEs presented here. Along track SLA observations distributed by CMEMS (<http://marine.copernicus.eu/>) referenced to an unbiased Mean Dynamic Topography (MDT) based on the CNES/CLS 2013 MDT are used. Gridded satellite SST OSTIA observations Level 4 (L4: SST analysis using optimal interpolation (OI) on a global 0.054 degree grid) are assimilated each week in addition to SST measurements from the in situ database delivered by the CORIOLIS centre (<http://www.coriolis.eu.org/>). Assimilation of in situ temperature and salinity profiles from this database are from Argo floats, XBT, CTDs, moorings, gliders and sea mammals. The assimilation of those routine observations in the OSEs provides a realistic context for the global ocean observing system so that the experiments address the complementarity of the different data sets with satellite SSS. The only exception is the TAO mooring observations of salinity that are withheld from the analysis and kept as independent observations to evaluate the performance of the assimilation experiment and the impact of the SSS assimilation. The SSS in the real time system is only constrained at large scale by in-situ observations, mostly Argo floats that usually start to measure at 5 meters depth.

2.2.2 SSS from space

In this study, we assimilate a SMOS Level 3 (L3: provided on a grid, but with no in-filling) SSS product at 0.25° resolution. L3 products are qualified (quality controlled) and processed at the Data Production Center (CPDC) of the Centre Aval de Traitement des Données SMOS (CATDS CEC-LOCEAN) (Boutin et al., 2017). Compared to Level 2 products (L2: SSS values at the native swath resolution) they benefit from additional corrections. These are 18-day products sampled at 25km resolution provided every 4 days (the precise description of the time filtering is in the documentation at <http://www.catds.fr/Products/Available-products-from-CEC-OS/L3-Debiased-Locean-v2>). We have checked that this temporal resolution fits well the model resolution and the weekly analysis window. In practice, the gridded SSS which is the closest to the analysis date (the fourth day of the week) provides the SSS data for the cycle. The model counterpart is the time average over the cycle. Due to a low signal to noise ratio, the assimilation of the SSS data is limited in the latitudinal band between 40°S and 40°N .

2.3 Data Assimilation Scheme

The assimilation scheme implemented in the real time Mercator Ocean systems is based on a reduced order Kalman Filter called SAM2 (Système d'Assimilation Mercator V2) and is described in Lellouche et al., (2013) and Lellouche et al., (2018).

2.3.1 Background Error Covariances

The SAM2 system uses a background error covariance matrix based on a reduced basis of multivariate model anomalies built from a fixed collection of model anomalies. The anomalies are computed from a previous simulation for a period of 8 years with the in-situ bias correction, detailed in the section 2.3.3. The forecast error covariances rely on a fixed basis, seasonally variable ensemble of anomalies calculated from this long experiment. A significant number of anomalies are kept from one analysis to the other, thus ensuring error covariance continuity. The aim is to obtain an ensemble of anomalies representative of the error covariance (Oke et al., 2008), which provide an estimate of the error on the ocean state at a given period of the year. The localization of the error covariance is performed assuming a zero-covariance beyond a distance defined as twice the local spatial correlation scale. These spatial correlation scales are also used to select the data around the analysis point. The model correction (analysis increment) is a linear combination of these anomalies. This correction is applied incrementally over the assimilation cycle temporal window using an incremental analysis update, see (Bloom et al., 1996; Benkiran and Greiner 2008).

2.3.2 Observation Error Covariances

The observation errors specified in the assimilation scheme are assumed to be uncorrelated with each other. Observation errors include representativity errors specified as a fixed error map and an instrumental error. Representativity errors concerning in situ observations were calculated a posteriori from a reanalysis over the period 2008-2012. The method (Desroziers et al.,

2005) consists of the computation of a ratio, which is a function of observation errors, innovations and residuals. These estimated errors are constant throughout the year.

The instrumental errors of SLA, SST and in situ measurements are summarized in Table 1. Fig. 2a shows the representativity error used for the in-situ SSS and an example of the resulting salinity error (Fig. 2b) for in-situ data for the week 20-27 January 2016. The SSS error from space used in the is detailed in SAM2 (2.5 and estimated during the bias correction scheme procedure.

2.4 Bias correction scheme

2.4.1 Bias correction scheme for large scale 3D temperature and salinity: in-situ T/S

Contrary to sea level anomalies data, biases between model and data exist for subsurface quantities such as temperature and salinity. As with the time-varying error components, such biases can often be related to the use of a coarser grid for data or to systematic errors in the forcing (Leeuwenburgh, 2007).

As written in Lellouche et al., (2013), a 3DVar bias correction is applied for large scale 3D temperature and salinity fields. The aim of this bias correction is to correct the large-scale, slowly evolving errors of the model, whereas the SAM assimilation scheme is used to correct the smaller scales of the model forecast error.

This is applied separately to the model's prognostic T/S equations from in-situ profile innovations calculated over the preceding month on a coarse grid ($1^\circ \times 1^\circ$). This bias is the minimizer of the cost function given by the Eq. 1.

$$J(\mathbf{x}) = \frac{1}{2} \mathbf{x}^T \mathbf{B}^{-1} \mathbf{x} + \frac{1}{2} (\mathbf{d} - \mathbf{H} \mathbf{x})^T \mathbf{R}^{-1} (\mathbf{d} - \mathbf{H} \mathbf{x}) \quad (1)$$

where $\mathbf{d} = \langle \text{Salinity}_{in-situ} \rangle - \langle \text{Salinity}_{model} \rangle$ for salinity field

\mathbf{d} is the innovation vector of T/S, i.e the mean ($\langle \rangle$) innovation of in-situ T/S over 1 month in a $1^\circ \times 1^\circ$ grid boxes. \mathbf{x} is the temperature or salinity in-situ bias to estimate, \mathbf{B} denotes the background error covariance of the 3D bias, \mathbf{d} is the innovation vector, \mathbf{H} is the observation operator, \mathbf{R} is the observation covariance error. The vertical grid is a coarse grid (only 23 levels) which is different of the model vertical grid (50 levels). For example, the in-situ innovation at sea surface for T/S is calculated from the average of model and observations between 0 and 11 meters depth. Because temperature and salinity biases are not necessarily correlated at large scales, these two variables are processed separately. Spatial correlations in \mathbf{B} are modeled by means of an anisotropic Gaussian recursive filter (Wu et al., 1992; Riishøjgaard, 1998; Purser et al., 2003). Finally, bias correction of T, S and dynamic height are computed and interpolated on the model grid and applied as tendencies in the model prognostic equations with a 1-month time scale.

2.4.2 Bias correction scheme for large scale SSS large: SSS from space

Earlier attempts to assimilate SSS data have shown the importance of using unbiased satellite SSS data while implementing rigorous quality control in an upstream process (Tranchant et al., 2015). In this study, the bias control of satellite SSS has

been modelled by modifying the current T/S bias (in-situ) correction 3Dvar cost function (Eq. 1). An extra term to take into account biases in the satellite SSS data has been added and denoted ξ in the 3DVar cost function (Eq.2). The new SSS bias is the minimizer of the cost function given by the Eq. 2.

$$J(\mathbf{x}, \xi) = \frac{1}{2} \mathbf{x}^T \mathbf{B}^{-1} \mathbf{x} + \frac{1}{2} (\mathbf{d} - \mathbf{H} \mathbf{x})^T \mathbf{R}^{-1} (\mathbf{d} - \mathbf{H} \mathbf{x}) + \frac{1}{2} \xi^T \mathbf{B}_{\xi}^{-1} \xi + \frac{1}{2} (\mathbf{d}_{\xi} - \mathbf{H} \xi)^T \mathbf{R}_{\xi}^{-1} (\mathbf{d}_{\xi} - \mathbf{H} \xi) \quad (2)$$

where $\mathbf{d}_{\xi} = (\langle \text{SSS}_{SMOS} \rangle - \xi) - \langle \text{SSS}_{model(0.5m)} \rangle$

Here, \mathbf{d}_{ξ} is the innovation of SSS bias at surface, i.e the mean ($\langle \rangle$) innovation of SMOS SSS over 1 month on a $1^\circ \times 1^\circ$ grid.

To get an optimal set of parameters (weights, spatial scales and errors), several estimations were performed with data withdrawing. In Fig. 3, examples of salinity bias near the surface (\mathbf{x}) without (a) (Eq.1) and with (c) (Eq. 2) the SSS bias term (ξ) are shown. The patterns are similar except at the equator where the SSS bias (Fig3b) influences the bias correction of salinity (Fig 3c) with smaller scales. There may also be opposite sign but amplitudes are the same. In this example, a persistent large innovations at several depths (11m, 41 m and 79 m) (not shown here) may induce a larger bias of salinity (negative anomaly) at sea surface near $120^\circ\text{W}/20^\circ\text{S}$.

2.5 SSS observation error

The Desroziers diagnostic (Desroziers et al., 2005) is commonly used for estimating observation error statistics and is used here to adapt the observation error from the background and analysis residuals calculated in the bias correction, see also (Lellouche et al., 2018). Following Desroziers et al., (2005), the observation error of the bias \mathbf{R}_{ξ} is optimal when is equal to the statistical expectation of the cross-product between the residual \mathbf{d}_{ξ}^a and the innovation \mathbf{d}_{ξ} of the SSS bias, see Eq. 3.

$$\mathbf{R}_{\xi} = E [\mathbf{d}_{\xi} \mathbf{d}_{\xi}^a] \quad (3)$$

Actually, \mathbf{R}_{ξ} is estimated iteratively (n=5) by an iterative boot-strap method computed on a $3^\circ \times 3^\circ$ grid. Five successive analyses are made followed by five estimates of the Desroziers ratio \mathbf{r}_{ξ}^i expressed as Eq. 4 for an analysis i.

$$\mathbf{r}_{\xi}^i = \frac{E [\mathbf{d}_{\xi} \mathbf{d}_{\xi}^{a_i}]}{\mathbf{R}_{\xi}^i} \quad (4)$$

From an observation error a priori \mathbf{R}_{ξ}^0 and by the successive ratio $\mathbf{r}_{\xi}^{i=1,n}$, we obtain Eq.5:

$$\mathbf{R}_{\xi} = \mathbf{r}_{\xi}^1 \dots \mathbf{r}_{\xi}^n \mathbf{R}_{\xi}^0 \quad \text{with } \mathbf{r}_{\xi}^{i=1,n} = \frac{E [\mathbf{d}_{\xi} \mathbf{d}_{\xi}^{a_i}]}{\mathbf{R}_{\xi}^{i=1,n}} \quad (5)$$

The a priori error \mathbf{R}_{ξ}^0 is a combination of a zonally varying error, together with an increase over regions with sparse in-situ data and near the coast. This increase varies with the cycle. It means that the SSS bias could not be estimated accurately in the absence of in situ data, and hence will have no impact in the assimilation in those regions void of in situ data. Fig. 4 shows an

example of the final Desroziers ratio r_{ξ}^5 . It illustrates how the fixed zonal error is increased near the equator and reinforced near central America where in situ data are sparse. There is also a local increase near Samoa (170°W-13°S), probably due to RFI pollution. Several simulations have been done with and without bias correction in order to check the validity of the estimated SSS errors in the data assimilation scheme SAM2.

- 5 Finally, for each weekly analysis, the total observation error of satellite SSS (SMOS) prescribed in the data assimilation scheme is the maximum of the above observation error estimated during the bias correction process and the measurements error ($R_{instr.}$) supplied by the data producers (used as a threshold) , see Eq. 6. These measurement error estimates bring smaller scales than can be estimated by the Desroziers diagnostic.

$$R_{Tot} = \max(R_{\xi}, R_{instr.}) \quad (6)$$

10 2.4 OSE design

- Two parallel simulations were produced, the REF experiment and the SMOS experiment (hereafter SMOSexp) see Table 2. The only difference is the assimilation of the SSS SMOS observations. Both experiments begin in January 2014 from the same initial conditions coming from a previous reanalysis using only the bias correction of T/S without any data assimilation. The period covers the onset and development of the El-Niño 2015 event. The length of the OSE should at least cover one year, more if possible, as it takes 3 months for the system to be in equilibrium with the new data assimilated. This “adjustment” period is longer for observations deeper in the ocean (below the thermocline). Here, up to 2-year simulations are analyzed (2014-March2016).

- The comparison between the two simulations highlights the impact of the SSS data assimilation on the ocean circulation and the comparison to the other observations (independent or not) will allow us to verify the coherency between the different observation networks and the way they are assimilated.

3. OSE analysis

- Different diagnostics are now used to assess the impact of SSS data assimilation on the analysed model fields. First the analysis from the REF and SMOSexp simulations are evaluated against the assimilated observations. Then, the 3D fields of the simulations with and without SSS data assimilated are compared and the changes in the surface and subsurface fields are analysed. Finally, TAO/TRITON array salinity observations which are deliberately with-held and delayed time ThermoSalinoGraph (TSG) which are not assimilated in the analysis of all experiments are used to conduct independent analysis observation comparison. The analysis focuses on the tropical Pacific region during the Niño 2015 event.

3.1 Assessment of the misfit reduction based on the data assimilated in the analysis

3.1.1 Assimilation diagnostics

The REF and SMOSexp simulations differ only by assimilating satellite SSS data (Table 2). We first check the success of the assimilation procedure in reducing the misfit from the assimilated SSS observations within the prescribed error bar. We then look at the Root-Mean-Square (RMS) of in-situ salinity observation innovations near 6 meters depth in both simulations. The model forecast range used in this comparison is from 1 to 7 days.

Fig. 6 shows the time-series of Root-Mean-Square Errors (RMSEs) between the model near-surface salinity (6 m depth) compared to in situ observations (dotted lines) and between the model SSS (0.5 m depth) compared to the bias-corrected SMOS SSS (solid lines) for both simulations (REF in black, SMOSexp in red). As expected, the SMOS SSS data assimilation clearly leads to a significant reduction in the innovations of the SMOS data. Global, Tropical Pacific (and central Pacific (Niño3.4) regional statistics are shown. The global RMSE to SMOS data is around 0.28 pss (practical salinity scale) in the reference simulation and reduced to 0.21 pss when debiased SMOS data are assimilated, corresponding to an error reduction of 24%. This shows that the combination of bias correction and data assimilation perform well. The innovation of the in-situ salinity observations is also slightly reduced by 5%. This shows that the assimilation of SMOS SSS observations do not introduce overall incoherent information and reduce the misfit to the in-situ observations. It also confirms that SSS errors estimated in the bias correction procedure and used in the assimilation scheme are well tuned and the data bring coherent information. Consequently, large scales biases are removed well. **SPEAK ABOUT WESTERN PACIFIC it is better SAYS ABOUT absolute rmse** Similar results are found for all the Tropical regions with a SMOS SSS RMSE reduction of 25%, and an in-situ salinity RMSE reduction of 5%, see Table 3. It should be mentioned that the number of in situ salinity observation per week is not always sufficient to ensure robust statistics in small regions.

Time series and maps of the misfits between observation and model forecasts are complementary to analyse the temporal and spatial variability of the model observation differences. Fig. 7 shows the mean and root-mean-square differences of daily mean SSS in the analysis fields in REF and SMOSexp compared to the original (non-debiased) SMOS data over the year 2015 for the Tropical Pacific Ocean.

The mean SSS bias in REF exhibits large scale patterns, coinciding with the 2015 SSS anomaly for the open ocean (Fig. 1). Large bias is also found in the Indonesian Archipelago. In contrast, the bias is effectively reduced in SMOSexp as well as the root-mean-square differences that is reduced to less than 0.2 PSS (black isohaline) in most of the Tropical Pacific Ocean.

Assimilation of surface salinity observations from satellite has a slight impact on subsurface salinity fields. The mean RMSE and the percentage of RMSE difference of the salinity profiles (mainly from Argo floats) are computed over the entire period and the global domain (Fig. 8). There is a slight decrease in the first 20 meters below the surface when SSS data are assimilated additionally to in situ salinity data. It shows that the additional information brought by the SSS is in agreement with the salinity in situ observation close to the surface. It can even help improving the global salinity representation in the first 20 meters by better constraining the model forecast with the satellite SSS.

In situ temperature innovations in the global domain as well as in the Tropical Pacific region do not show significant changes. The same is found for SLA (SALTO/DUACS along track) and SST innovations (OSTIA L4). SSS data assimilation has a quite-neutral impact on the innovations associated with those observations.

3.1.1 Impact of assimilating SMOS data during El-Niño 2015/16

5 We now look at the changes in the analysed surface and subsurface fields due to the SSS data assimilation by comparing the 3D analysis of the REF and SMOSexp experiments. At basin scale, the REF simulation already agrees well with the 2015 mean deduced from the “unbiased” CATDS SMOS observations (Fig. 9). SMOS data assimilation induced changes in the order of 0.2 pss. It tends to weaken the salinity negative anomaly represented in the REF simulation within the ITCZ and SPCZ regions. This is in agreement with (Kidd et al., 2013) that show an overestimation of the ECMWF precipitation in the tropics compared to satellite observations. Elsewhere, the SMOS data assimilation increases the salinity. Large changes also occurred in the coastal zones (Indonesian archipelago and Central America coast), even if the specified error on SSS data was larger in those regions than in the open ocean.

The associated vertical salinity changes to the SMOS SSS data assimilation at the equator are represented on Fig. 10. The largest magnitudes (saltier) are found in the first 50 m depth and along the coastal bathymetry, elsewhere changes are very small, less than 0.05 pss. Overall, at the equator (excepted in coastal areas), the data assimilation of SMOS SSS leads to fresher waters in the East and saltier waters in the West for the year 2015.

The highest variability of the surface salinity at monthly scale during the year 2015 is found within the ITCZ, SPCZ and in the Eastern Pacific fresh pool, in both simulations and SMOS observations (not shown). SMOS assimilation decreases the intensity of the variability of the SSS, in agreement with the observed variability. In summary, the SSS assimilation acts to counteract the precipitation excess, with a visible result on the salinity both in terms of time mean but also in term of variability.

During the Niño2015 event, a strong salinity anomaly pattern developed in the Tropical Pacific (Gasparin et Roemmich 2016), see also Figure 1. This anomaly corresponds to the ITCZ and SPCZ areas. Fig. 11 shows the evolution of the SSS at 5°N, the latitude where the salinity anomaly is the largest (Hackert et al., 2014). Both the REF and SMOSexp simulations represent the decrease in time of the salinity peaking in fall 2015 at this latitude, for the longitude between 160°E and 120°W. Note that this salinity anomaly is lower in the SMOS data (SMOS SSS is saltier) with a smaller extent. The Eastern freshwater pool extended further west during 2015, but it was fresher in the REF simulation compared to the SMOSexp experiment.

While the impact of SSS assimilation is neutral on the other variables (temperature and SSH) in terms of data assimilation diagnostics (RMSE), it is not the case at seasonal time scales.

SSS data assimilation has also an impact on the other surface variables. SST differences at 5°N and velocity differences at the equator are represented on Fig.12. The differences are mainly associated with the wave propagation seen in all the surface fields. In the freshwater pool, the SMOS data assimilation weakens the freshening and induces a slight warming of about 0.05°C (Fig12b). At the equator, the zonal eastward advection is enhanced (positive pattern at the east of the date line) from January to October 2015 (Fig.12c) which has the effect of helping the Warm Water Pool migration to the east. This effect is

known to promotes the ocean-atmosphere coupling and thus the triggering of El Niño. In the Eastern basin, there is also an increase of the westward propagation during Autumn 2015 that are possibly linked to the increase of Tropical Instability Waves (TIWs), see Figure 13.

Another effect of SSS changes can be viewed on Barrier layers which are quasi-permanent in the Tropical Pacific. Barrier Layer Thickness (BLT) can influence the air-sea interaction, ocean heat budget, climate change and onset of ENSO events, (Maes et al., 2002; Maes et al., 2004). The barrier layer acts as a barrier to turbulent mixing of cooler thermocline waters into mixed layer and thereby plays an important role in the ocean surface layer heat budget (Lukas and Lindstrom, 1991). The Hovmöller diagram of BLT at 5°N is shown on Figure 13 for both experiments. It shows the occurrence of thick BLT in the eastern Pacific ([130°W – 140°W]) in September to November which corresponds to measurements taken during strong El Niño events (Mignot et al., 2007). Note also that the eastward displacement of the thick barrier layer has already been observed during previous El Nino events, see Qu et al., (2014).

From Figure 12a and Figure 13, we show that the Eastern and Central Pacific are saltier in the SMOSexp experiment which induce a decrease of the stratification and then a decreased BLT. This effect could also induce a mixing enhancement that could be also enhanced by TIWs activity. From a long-term TAO mooring record at 0°N 140° W, Moum et al., (2009) suggest that mixing may always be enhanced during the passage of TIWs. Consequently, even if TIWs are less active during a El-Nino phase than in a La Nina phase, it was interesting to investigate the TIW propagation signature in SSH. Moreover, Yin et al., (2014) and Lee et al., (2012) show also the capability of monitoring TIWs by Aquarius and SMOS data. Lyman et al., (2007) show that 33-day TIWs are associated with the first meridional mode Rossby wave. Hovmöller of daily anomalies of SSH at 4°N filtered at 33 days are shown in Fig. 14. For both experiments, the westward propagation of TIW is shown in the Eastern part of the basin. A reinforcement of the TIWs in the Central Pacific near 140°W (the slope is steeper) appears during the second half of 2015 in the SMOSexp experiment (0.35 m/s) compared to the REF experiment (0.25 m/s). As mentioned above, this could be correlated to the decrease of BLT, see Figure 13. On the contrary, a weakening of TIWs appears during the August-September period in the eastern part of the basin for the SMOSexp experiment. The same kind of impact have been shown recently in Hackert et al., (2014) for the initialization of the coupled forecast, where a positive impact of SSS assimilation is provided on surface layer density changes via Rossby waves. They also show that these density perturbations provide the background state to amplify equatorial Kelvin waves and ENSO signal.

3.2 Evaluation of the analysis toward independent observations

We now compare the analysed fields to independent observations, i.e. withheld from all assimilation experiments. This will allow verifying that the changes in the physical fields induced by the SMOS data assimilation are in agreement with external sources of information. For this purpose, the TAO mooring (salinity) observations and the reprocessed TSG data from the French SS Observation Service were withheld from all experiments. This is therefore a fully independent validation.

3.2.1 Comparisons to TAO mooring

TAO moorings deliver high frequency measurements at fixed locations. Such platforms allow us to look at high frequency variability that is not captured by drifting platforms. The hourly analysed salinity is collocated at the TAO mooring positions for the REF and SMOSexp simulations. Fig. 15 shows the time evolution of TAO salinity observations (valid at 1 m depth) at three mooring locations in the equatorial Pacific (warm pool, cold tongue and salt front) compared to the model (analysis) for the REF and SMOSexp OSE experiments at the first level (~0.5 m depth). Assimilated SMOS data have also been added. In this example, the salinity evolution of the REF experiment (in green) appears less correlated with the TAO salinity mooring observations (black dots). The SMOSexp simulation shows a better agreement, except for some strongly variable events. The differences between the SMOSexp simulation and TAO non-assimilated observations are most of the time less than 0.1 pss. The high frequency variability seen in the observations is also reproduced in the assimilative simulations, with a better agreement when SMOS data are assimilated, except during some specific periods. Tang et al., (2017) also found some disagreement between the TAO observations and SMAP/SMOS observations and Argo analysis during short periods. There is an improvement in the cold tongue during the end of summer, in fall 2015 and during the last 2 months of the SMOS simulation (15a) in the region where the data assimilation of SMOS reduces the freshening. Globally, an improvement occurs also in the warm pool (15b) over the entire period. One interesting feature is that when TAO mooring data are missing during a long period near the salt front, the SSS from the SMOSexp experiment is different but closer to TAO mooring when measurements come back, Fig. 15c. Obviously, the assimilated 4-days SMOS data are smoother but are able to capture the large scale variability. This also shows the level of accuracy we need to capture higher variability. The precipitation rate superimposed on the SSS proves that it is not the only process that plays a role in the salinity variability. Indeed, a high precipitation rate does not induce necessarily a strong freshening at the sea surface where advection, vertical mixing and SSS SMOS data assimilation can counteract its effect. This also shows that the observation error should not be increased locally depending on the precipitation.

These three examples show a positive impact but it is also interesting to have a global view of all TAO moorings over the 2015/2016 El-Niño event. As in (Martin et al., 2018), Fig. 16 shows the differences in RMSD from hourly TAO mooring salinity values at 1 m depth calculated over the period 1st Jan 2014 to 16th March 2016. The impact of the SMOS assimilation is contrasted by showing negative (positive) values which indicates that it reduces (increases) the RMSD. The impact is positive and more significant in the western Tropical Pacific near the dateline and in the western Pacific up to 5°N. The impact is quite neutral and even negative in the eastern tropical Pacific (140°W-110°W) between 2°S and 2°N where generally (i) the SMOS bias is larger (Fig. 4b), (ii) there are few in-situ SSS data (Fig. 2) and (iii) where the observation error is larger (Fig. 5). Actually, the impact of SMOS SSS assimilation is larger in the ITCZ and SPCZ regions as shown also in the Fig. 9d. This reflects the overestimation of E-P that the data assimilation tends to correct and the SMOSexp experiment is saltier in regions where precipitation is higher. Finally, during the El-Niño 2015/2016 event, there is a small positive impact overall from the SMOS assimilation with a reduction in RMSD from 0.326 to 0.316 pss (about 3%).

3.2.1 Comparisons to ship SSS

Post processed TSG observations from the French SSS Observation Service (SSS-OS; (<http://www.legos.obs-mip.fr/observations/ssss>)) were collected along the routes of voluntary merchant ships, see Alory et al., 2015. The SSS estimates have a ~2.5 km resolution along the ship track with an estimated error close to 0.08 pss. Salinity analysed fields from REF and SMOSexp simulations are collocated to the TSG observations. Salinity observations from vessel mounted thermosalinographs allow validation of the short time and space scales of near surface salinity. Two ship routes (Fig. 17) that cross the Tropical Pacific Ocean in June 2015 are chosen to verify that salinity changes when SSS SMOS data are assimilated are in agreement with such observations.

Fig. 17 shows the comparison between the TSG salinity observations (in red) along the Matisse ship route collocated with the REF (black dashed line) and SMOSexp (black line) salinity analyzed fields. The variability of the SSS measurements, lower than the daily frequency, is well represented in both simulations with only small differences of less than 0.2 pss except in the freshwater on the eastern part of the basin. In this region, the salinity dropped down to less than 34.0 PSS. The REF simulation differs from the TSG data by more than 0.5 pss within the freshwater pool, marked by a very sharp salinity front. The SMOSexp simulation shows a much better agreement with the SSS from the TSG observations: even if the differences remain large, the misfit is reduced.

This confirms once again that the weakening of the freshening in the freshwater pool in the eastern Pacific induced by the SMOS data assimilation is realistic, as it is seen by different in situ observation platforms.

4. Discussion and conclusions

The L3 SMOS CATDS data used in this study is considered as an “unbiased” product. Yet, they still contain some residual biases that must be removed prior to bias correction and data assimilation. It was one of the major challenge of this study: to estimate the residual SSS bias, and to estimate a suitable observation error for the data assimilation system. It was made possible using an analysis of the residuals and errors with a statistical technique (Desroziers et al., 2005). The “debiased” data could then be assimilated by the SAM2 assimilation scheme which relies on the unbiased hypothesis. The bias estimated by the ocean forecasting system can also be used to correct the L3 SMOS CATDS data for other purposes.

The system was carefully tuned and tested to efficiently assimilate the new SSS observations before running the longer simulations that are analyzed here. The proper specification of the observation operator and error covariance matrix were also based on discussions with the data provider. This study helped us to progress in the understanding of the biases and errors that can degrade the SMOS SSS performance.

Nevertheless, there is still room for improvement. For instance, we used a zonal error as input to the error estimation with the Desroziers technique. It could be beneficial to take into account the smaller scales linked to a shallow stratification that arises with strong precipitations and/or river runoff.

The SMOS data need accurate in-situ data (not only at the surface) to correct their own biases and estimate a suitable error (including data/system representativity). When enough data is available, SMOS really acts as a gap filler. There is a clear impact on the scales about 1° - 2° . This can be seen on the Fig. 12 (Hovmöller), and additional spectral analyses (not shown) confirm this finding. So, it is important for future satellite SSS to provide a good accuracy in this band. It also shows that background error correlation length-scales used in the bias correction scheme could be optimized by improving the in-situ network and the SSS SMOS accuracy.

Globally, the SSS data assimilation slightly improves the simulation compared to a simulation assimilating only observations of in situ, SST and SLA data. It highlights that no incoherent information was brought by the SSS data compared to the other assimilated observations. When looking at the impact of the SMOS SSS assimilation, we found a positive impact in salinity with respect to in-situ data over the top 30 meters. The root mean square error (RMSE) of in-situ surface salinity is reduced in all regions of the Tropical Pacific. The impact varies depending on the region and can reach 10% in the North Tropical Pacific where the SSS anomaly is the strongest. Comparisons to independent TAO/Triton data corroborate the fact that the impact of SMOS SSS assimilation is larger in the ITCZ and SPCZ regions. This also reflects that the overestimation of E-P is corrected by data assimilation through salting in regions where precipitations are higher.

There is a few impact on the SST. For instance, the area of the SST warmer than 28.5°C was little affected. It means that the local impact on the air-sea coupling is negligible. But, an impact on SSH have been seen through TIWs which have been reduced and then strengthened in the eastern part of the basin during the last half of the 2015 year. The wave activity can be linked to the Barrier Layer Thickness which has also been impacted through a positive feedback. Another result can be seen on the strengthened Eastward advection of the warm pool in 2015 (Fig. 12, Hovmöller of zonal velocity difference). It means that SMOS SSS assimilation has a non-local impact on the ocean-atmosphere dynamics. These findings are close to those of Hackert et al., (2014) with a global ocean-atmosphere coupled model but benefits in term of seasonal forecasting have still to be quantified.

The next step will be to assimilate SSS from space at higher latitudes where low sea surface temperature (SST) degrades the brightness temperature sensitivity to SSS (Sabia et al., 2014). A longer ocean reanalysis with continuously improved SSS SMOS (available for over 9 years) and SMAP (available since 2015) data could bring new information on the water cycle.

The focus of this study was on the tropical Pacific. But the system is global, and, in spite of RFI pollution near some coasts, we found clear improvements near the Amazon, Rio Del Plata, ... So, the benefit from assimilating SMOS SSS is not restricted to the equatorial band. Its positive impact near the mid-latitudes major rivers is a chance to better monitor the strengthening of the water cycle (Durack, 2015).

Acknowledgements

We gratefully acknowledge funding from ESA as part of the SMOS-Niño15 project, coordinated by C. Donlon. We also thank the providers of the datasets used here. J. Boutin (LOCEAN/CATDS) provided the SMOS data and provided useful inputs to understand the nature of the SMOS bias estimates. Sea surface salinity data derived from voluntary observing ships were collected, validated, archived, and made freely available by the French Sea Surface Salinity Observation Service (<http://www.legos.obs-mip.fr/observations/sss/>). Thanks to the GTMBA Project Office of NOAA/PMEL to provide TAO/TRITON mooring data. We would also like to acknowledge Matthew Martin (MetOffice) for his careful reading of the manuscript and his comments which were very helpful. We would also like to acknowledge the contribution of the two anonymous reviewers whose suggestions improved this paper significantly.

References

- Alory, G., Delcroix, T., Téchiné, P., Diverres, D., Varillon, D., Cravatte, S., Gouriou, Y., Grelet, J., Jacquin, S., Kestenare, E., Maes, C., Morrow, R., Perrier, J., Reverdin, G., Roubaud, F., The French contribution to the voluntary observing ships network of sea surface salinity. *Deep-Sea Res.* 105, 1–18. <http://dx.doi.org/10.1016/j.DSR.2015.08.005>, 2015.
- Ashok, K., and T. Yamagata, The El Niño with a difference. *Nature*. 461, 481–484, 2009.
- 15 Barnston AG, Chelliah M, Goldenberg SB. 1997. Documentation of a highly ENSO-related SST region in the Equatorial Pacific. *Atmosphere-Ocean* **35**: 367–383.
- Benkiran, M. and E. Greiner, Impact of the Incremental Analysis Updates on a Real-Time System of the North Atlantic Ocean. *Journal of Atmospheric and Oceanic Technology* 25(11): 2055–2073, 2008.
- Bloom, S. C., L. L. Takacs, A. M. da Silva, and D. Ledvina, Data assimilation using incremental analysis updates. *Mon. Wea. Rev.*, 124, 1256–1271, [https://doi.org/10.1175/1520-0493\(1996\)124<1256:DAUIAU>2.0.CO;2](https://doi.org/10.1175/1520-0493(1996)124<1256:DAUIAU>2.0.CO;2), 1996.
- 20 Boutin, J., Vergely, J.L., Marchand, S., SMOS SSS L3 Debias v2 Maps Generated by CATDS CEC LOCEAN. <http://dx.doi.org/10.17882/52804>, 2017.
- Boutin, J., Chao, Y., Asher, W. E., Delcroix, T., Drucker, R., Drushka, K., et al. . Satellite and In Situ Salinity: Understanding Near-Surface Stratification and Subfootprint Variability. *Bulletin of the American Meteorological Society*, 97(8), 1391–1407.
- 25 <https://doi.org/10.1175/BAMS-D-15-00032.1>, 2016.
- Chakraborty, A., R. Sharma, R. Kumar, and S. Basu, A SEEK filter assimilation of sea surface salinity from Aquarius in an OGCM: Implication for surface dynamics and thermohaline structure, *J. Geophys. Res. Oceans*, 119, doi:10.1002/2014JC009984, 2014.
- Corbett, C. M., Subrahmanyam, B., & Giese, B. S., A comparison of sea surface salinity in the equatorial Pacific Ocean during the 1997–1998, 2012–2013, and 2014–2015 ENSO events. *Climate Dynamics*, 3513–3526. <https://doi.org/10.1007/s00382-017-3527-y>, 2017.
- 30

- Dai, A. and Trenberth, K. E.: Estimates of freshwater discharge from continents: latitudinal and seasonal variations, *J. Hydrometeorol.*, 3, 660–687, 2002.
- Dai A., Qian, T., Trenberth, K., and Milliman, J. D.: Changes in Continental Freshwater 31 Discharge from 1948 to 2004, *J. Climate*, vol. 22, p.2773-2792, 2009.
- 5 Desroziers, G., L. Berre, B. Chapnik, and P. Poli. Diagnosis of observation, background and analysis error statistics in observation space. *Quarterly Journal of the Royal Meteorological Society*, 131:3385–3396, 2005.
- Durack, P.J. Ocean salinity and the global water cycle. *Oceanography* 28(1):20–31, <https://doi.org/10.5670/oceanog.2015.03>, 2015.
- Fujii, Y., K. Ogawa, G. B. Brassington, K. Ando, T. Yasuda & T. Kuragano, Evaluating the impacts of the tropical Pacific
10 observing system on the ocean analysis fields in the global ocean data assimilation system for operational seasonal forecasts in JMA, *Journal of Operational Oceanography*, 8:1,25-39, DOI: 10.1080/1755876X.2015.1014640, 2015.
- Gasparin, F., and D. Roemmich, The strong freshwater anomaly during the onset of the 2015/2016 El Niño, *Geophys. Res. Lett.*, 43, 6452–6460, doi:10.1002/2016GL069542, 2016.
- Guimbard, S., Reul, N., Chapron, B., Umbert, M., & Maes, C., Seasonal and interannual variability of the Eastern Tropical
15 Pacific Fresh Pool. *Journal of Geophysical Research: Oceans*, 122, 1749–1771. <https://doi.org/10.1002/2016JC012130>, 2017.
- Good, S. A., M. J. Martin, and N. A. Rayner (2013), EN4: Quality controlled ocean temperature and salinity profiles and monthly objective analyses with uncertainty estimates, *J. Geophys. Res. Oceans*, 118, 6704–6716, doi:10.1002/2013JC009067.
- Hackert, E., Busalacchi, A. J., & Ballabrera-Poy, J., Impact of Aquarius sea surface salinity observations on coupled forecasts for the tropical Indo-Pacific Ocean. *Journal of Geophysical Research: Oceans*, 119, 4045–4067.
20 <https://doi.org/10.1002/2013JC009697>, 2014.
- Hasson, A., Puy, M., Boutin, J., Guilyardi, E., Morrow, R., Northward propagation across the tropical North Pacific Ocean revealed by surface salinity: how El Niño anomalies reach Hawaii? *J. Geophys. Res.* 123. <http://dx.doi.org/10.1002/2017JC013423>, 2018.
- Hilburn, K. A.: The passive microwave water cycle product, Technical Report number 072409, Remote Sensing
25 Systems, Santa Rosa, CA, 30 pp., available at: <http://www.remss.com> (last access: 20 September 2018), 2009.**
- Kao, Hsun-Ying & Yu, Jin-Yi., Contrasting Eastern-Pacific and Central-Pacific Types of ENSO. *Journal of Climate*. 22., 615-632. 10.1175/2008JCLI2309.1, 2009.**
- Kidd, C., Dawkins, E., and Huffman, G.: Comparison of precipitation derived from the ECMWF operational forecast model and satellite precipitation datasets, *J. Hydrometeorol.*, 14, 1463–1482, doi:10.1175/JHM-D-12-0182.1, 2013.
- 30 Köhl A, Sena Martins M, Stammer D., Impact of assimilating surface salinity from SMOS on ocean circulation estimates. *J. Geophys. Res.-Oceans*, 119, 5449-5464, doi: 10.1002/2014JC010040, 2014.
- Lellouche, J.-M., Le Galloudec, O., Drévilion, M., Régnier, C., Greiner, E., Garric, G., Ferry, N., Desportes, C., Testut, C.-E., Bricaud, C., Bourdallé-Badie, R., Tranchant, B., Benkiran, M., Drillet, Y., Daudin, A., and De Nicola, C.: Evaluation of global monitoring and forecasting systems at Mercator Océan, *Ocean Sci.*, 9, 57–81, doi:10.5194/os-9-57-2013.

- Lellouche, J.-M., Greiner, E., Le Galloudec, O., Garric, G., Regnier, C., Drevillon, M., Benkiran, M., Testut, C.-E., Bourdalle-Badie, R., Gasparin, F., Hernandez, O., Levier, B., Drillet, Y., Remy, E., and Le Traon, P.-Y.: Recent updates on the Copernicus Marine Service global ocean monitoring and forecasting real-time 1/12° high resolution system, *Ocean Sci.*, 14, 1093-1126, <https://doi.org/10.5194/os-14-1093-2018>, 2018.
- 5 Lea, D. J., Martin, M. J. and Oke, P. R., Demonstrating the complementarity of observations in an operational ocean forecasting system. *Q.J.R. Meteorol. Soc.*, 140: 2037-2049. doi: 10.1002/qj.2281, 2014.
- Lee, T., G. Lagerloef, M. M. Gierach, H.-Y. Kao, S. Yueh, K. Dohan, Tropical instability waves linked to sea surface salinity anomalies, vol 39, issue 12, DOI:10.1029/2012GL052232, 2012.
- Leeuwenburgh O., Validation of an EnKF system for OGCM initialization assimilating temperature, Salinity, and surface height measurements. *Mon Weather Rev* 135:125–139, 2007
- 10 Lukas R, Lindstrom E., The mixed layer of the western equatorial Pacific Ocean *J. Geophys. Res. Oceans* 96(S01): 3343–3357, 1991.
- Lyman, J. M., G. C. Johnson, and W. S. Kessler, Distinct 17- and 33-day tropical instability waves in subsurface observations, *J. Phys. Oceanogr.*, 37, 855–872, doi:10.1175/JPO3023.1, 2007.
- 15 Madec G.. NEMO Ocean Engine, Tech. Rep. 27, Pole de modelisation de IPSL, http://www.nemo-ocean.eu/About-NEMO/Reference-manuals/NEMO_book_3.6_STABLE.., 2016.
- Maes, C., J. Picaut, and S. Belamari, Salinity barrier layer and onset of El Nino in a Pacific coupled model, *Geophys. Res. Lett.*, 29(24), 2206, doi:10.1029/2002GL016029, 2002.
- Maes, C., J. Picaut, Y. Kuroda, and K. Ando, Characteristics of the convergence zone at the eastern edge of the Pacific warm pool, *Geophys. Res. Lett.*, 31, L11304, doi:10.1029/2004GL019867., 2004.
- 20 McPhaden, M. J., Timmermann, A., Widlansky, M. J., Balmaseda, M. A., & Stockdale, T. N., The curious case of the El Niño that never happened: A perspective from 40 years of progress in climate research and forecasting. *Bulletin of the American Meteorological Society*, 96(10), 1647–1665, 2015.
- Martin M. J., R. R. King, J. While and A. Aguiar, Assimilating satellite sea surface salinity data from SMOS, Aquarius and SMAP into a global ocean forecasting system, submitted to *QJRM*S, 2018.
- 25 Mignot, J., C. de Boyer Monte'gut, A. Lazar, and S. Cravatte, Control of salinity on the mixed layer depth in the world ocean: 2. Tropical areas, *J. Geophys. Res.*, 112, C10010, doi:10.1029/2006JC003954, 2007.
- Moum, J. N., R. C. Lien, A. Perlin, J. D. Nash, M. C. Gregg, and P. J. Wiles, Sea surface cooling at the equator by subsurface mixing in tropical instability waves, *Nat. Geosci.*, 2, 761–765, doi:10.1038/ngeo657., 2009.
- 30 Oke, P.R., G. Larnicol, Y. Fujii, G.C. Smith, D.J. Lea, S. Guinehut, E. Remy, M. Alonso Balmaseda, T. Rykova, D. Surcel-Colan, M.J. Martin, A.A. Sellar, S. Mulet & V. Turpin, Assessing the impact of observations on ocean forecasts and reanalyses: Part 1, Global studies, *Journal of Operational Oceanography*, 8:sup1, s49-s62, 2015.
- Oke, P.R., G. Larnicol, E.M. Jones, V. Kourafalou, A.K. Sperrevik, F. Carse, C.A.S. Tanajura, B. Mourre, M. Tonani, G.B. Brassington, M. Le Henaff, G.R. Halliwell Jr., R. Atlas, A.M. Moore, C.A. Edwards, M.J. Martin, A.A. Sellar, A. Alvarez, P.

- De Mey & M. Iskandarani, Assessing the impact of observations on ocean forecasts and reanalyses: Part 2, Regional applications, *Journal of Operational Oceanography*, 8:sup1, s63-s79, 2015.
- Oke, P. R., Brassington, G. B., Griffin, D. A., and Schiller, A.: The Bluelink Ocean Data Assimilation System (BODAS), *Ocean Model.*, 21, 46–70, 2008.
- 5 Purser, R. J., W.-S. Wu, D. F. Parrish, and N. M. Roberts, Numerical aspects of the application of recursive filters to variational statistical analysis. Part I: Spatially homogeneous and isotropic Gaussian covariances. *Mon. Wea. Rev.*, 131, 1524-1535, 2003a.
- Qu, T., Song, Y. T., & Maes, C., Sea surface salinity and barrier layer variability in the equatorial Pacific as seen from Aquarius and Argo. *Journal of Geophysical Research: Oceans*, 119(1), 15–29. doi:10.1002/2013jc009375, 2014.
- 10 Reul N., Fournier S., Boutin J., Hernandez O., Maes C., Chapron B., Alory G., Quilfen Y., Tenerelli J., Morisset S., Kerr Y., Mecklenburg S. and Steven Delwart, Sea Surface Salinity Observations from Space with the SMOS Satellite: A New Means to Monitor the Marine Branch of the Water Cycle, *Surveys in Geophysics*, p 1-42, DOI: 10.1007/s10712-013-9244-0, <http://link.springer.com/article/10.1007%2Fs10712-013-9244-0>, 2013.
- Riishøjgaard, L. P.: A direct way of specifying flow-dependent background error correlations for meteorological analysis systems. *Tellus*, 50A, 42-57, 1998.
- 15 Sabia, R., A. Cristo, M. Talone, D. Fernández-Prieto and M. Portabella, "Impact of Sea Surface Temperature and Measurement Sampling on the SMOS Level 3 Salinity Products," in *IEEE Geoscience and Remote Sensing Letters*, vol. 11, no. 7, pp. 1245-1249, doi: 10.1109/LGRS.2013.2290710, 2014.
- Seelanki V, Sreenivas P, Prasad KVS. Impact of Aquarius Sea-Surface Salinity Assimilation in Improving the Ocean Analysis Over Indian Ocean. *Marine Geodesy*, 41 (2), 144-158, doi: 10.1080/01490419.2017.1422817., 2018.
- 20 Tang, Wenqing; Fore, Alexander; Yueh, Simon; Lee, Tong; Hayashi, Akiko; Sanchez-Franks, Alejandra; Martinez, Justino; King, Brian; Baranowski, Dariusz., Validating SMAP SSS with in situ measurements. *Remote Sensing of Environment*, 200. 326-340. <https://doi.org/10.1016/j.rse.2017.08.021>, 2017.
- Toyoda T, Fujii Y, Kuragano T, Matthews JP, Abe H, Ebuchi N, Usui N, Ogawa K, Kamachi M., Improvements to a Global Ocean Data Assimilation System Through the Incorporation of Aquarius Surface Salinity Data. *Q. J. Roy. Meteor. Soc.*, 141 (692), 2750-2759, doi: 10.1002/qj.2561., 2015.
- 25 Tranchant, B., Greiner, E., legalloudec, O. And Letraon P.: Sea Surface Salinity Data Assimilation Improvement in a Global Ocean Forecasting System at 1/4° from SMOS and Aquarius Data, 2nd science SMOS conference, 25-29 May 2015, ESA-ESAC, (near Madrid) Spain, 2015.
- 30 Vinogradova, N. T., Ponte, R. M., Fukumori, I., & Wang, O. (2014). Estimating Satellite Salinity Errors for Assimilation of Aquarius and SMOS Data into Climate Models. *J. Geophys. Res.-Oceans*, 119 (8), 4732-4744, doi: 10.1002/2014JC009906.
- Von Schuckmann et al., The Copernicus Marine Service Ocean State Report, *Journal of Operational Oceanography*, <https://doi.org/10.1080/1755876X.2018.1489208>, 2018.

Verenstein, M., Hoffman, F., Oleson, K., and Levis, S., Community Land Model version 3.0 (CLM3.0) user's guide. Technical report, National Center for Atmospheric Research, 2004.

Wolter, K. and Timlin, M. S., Measuring the strength of ENSO events – how does 1997/98 rank?, *Weather*, 53, 315–324, 1998.

- 5 Wu, W.-S., R. J. Purser, and D. F. Parrish, Three-dimensional variational analysis with spatially inhomogeneous covariances. *Mon. Wea. Rev.* 130, 2905-2916, 1992

Yin, X., J. Boutin, G. Reverdin, T. Lee, S. Arnault, and N. Martin, SMOS Sea Surface Salinity signals of tropical instability waves, *J. Geophys. Res. Oceans*, 119, 7811–7826, doi:10.1002/2014JC009960, 2014.

10

15

20

25

30

35

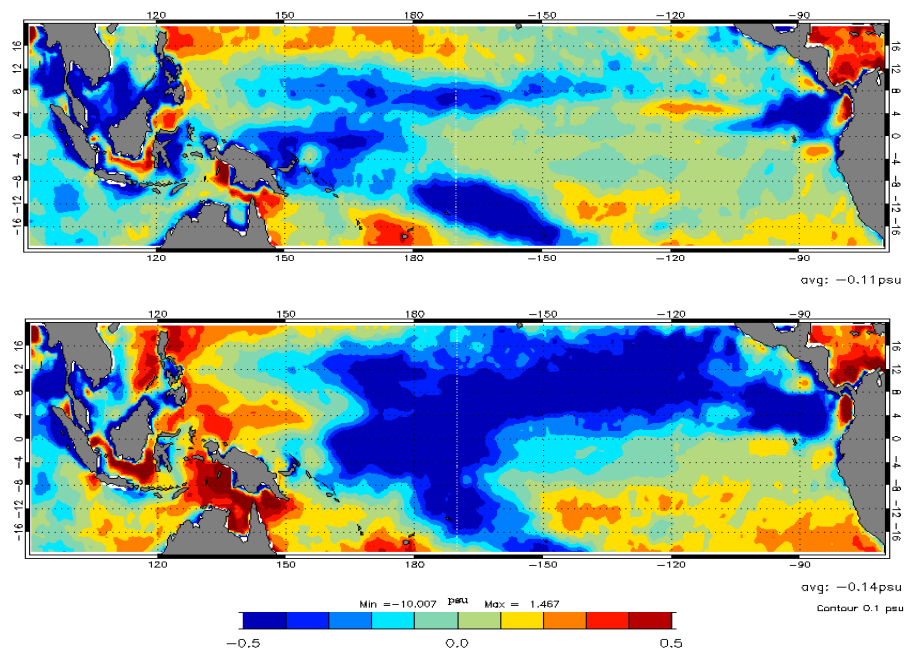


Figure 1: SSS anomalies (psu) in 2014 (top) and 2015 (bottom): mean salinity difference (model (control run) – WOA2013).

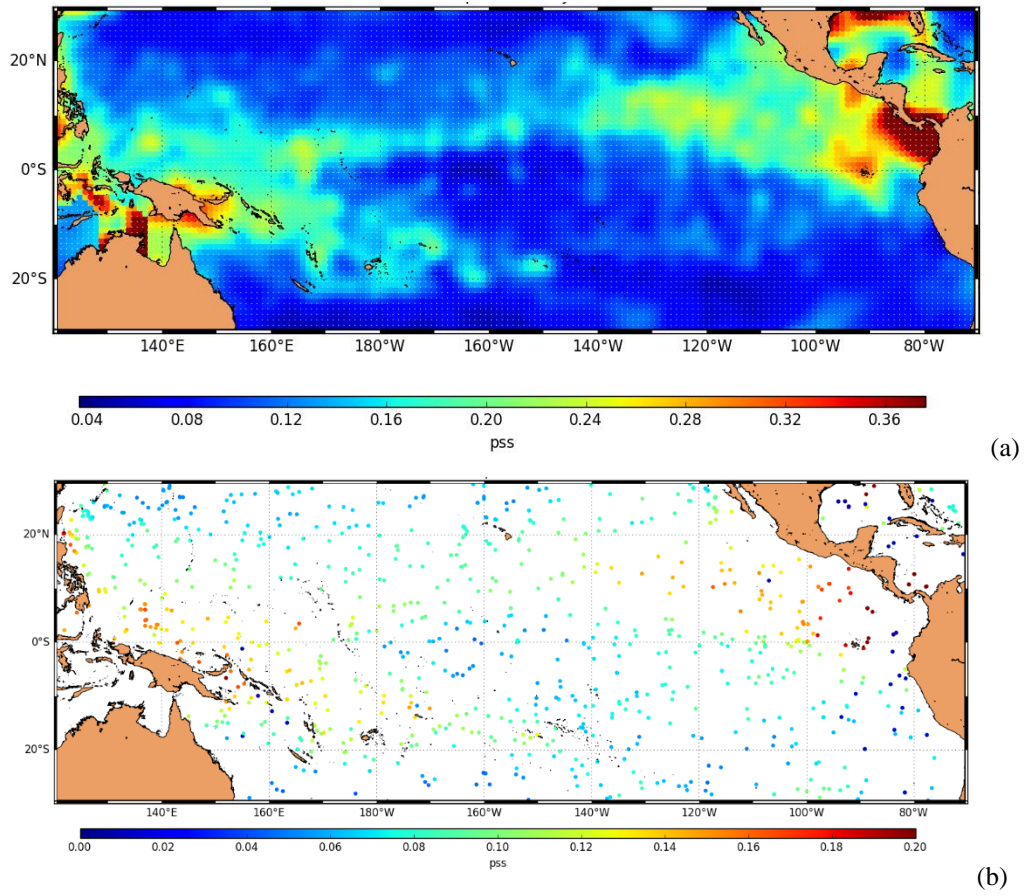


Figure 2: Representativity error of in-situ SSS ($R_{repr.}$) (a) and salinity error of in-situ data at sea surface (b) over the Tropical Pacific and used in the data assimilation system for the week 20-27 January 2016.

5

10

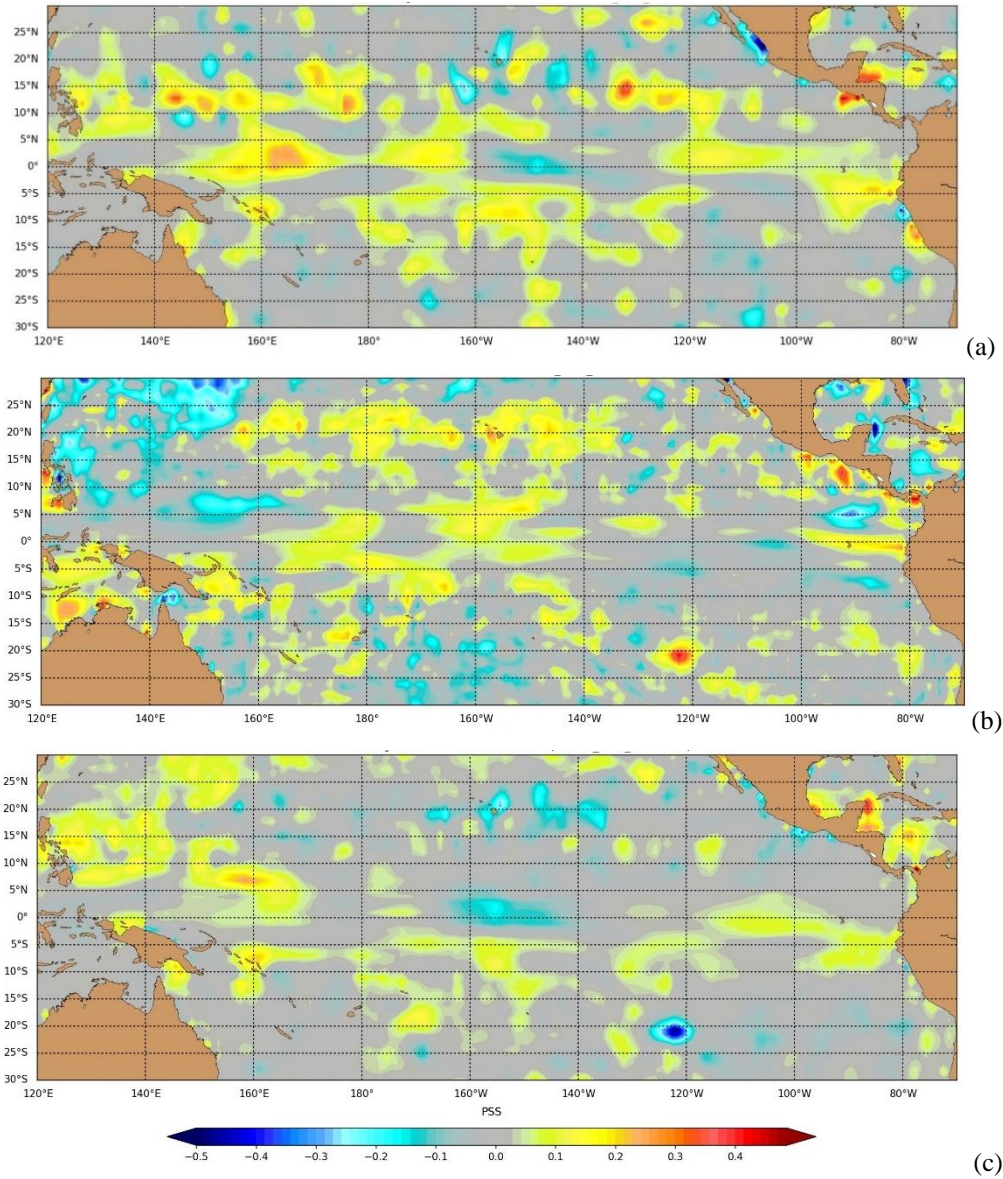


Figure 3: Example of model salinity bias (x) near the surface (Eq. 1a) calculated from in-situ data between 0 and 10 m depth only (a), of SSS bias (ξ) (Eq. 1b) calculated from in-situ data between 0 and 10 m depth and SMOS SSS (b) and salinity bias (x) (Eq. 1a + Eq. 1b) from in-situ data between 0 and 10 m and SMOS SSS (c) in the Tropical Pacific (week 20-27 January 2016).

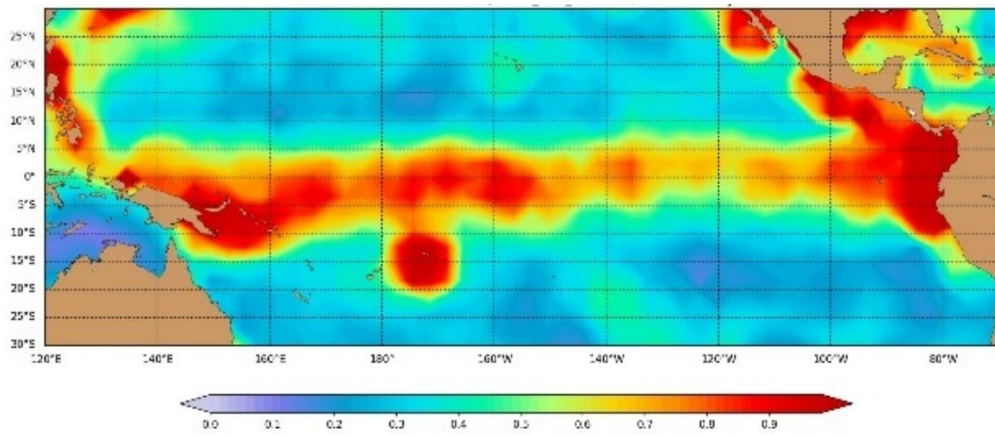
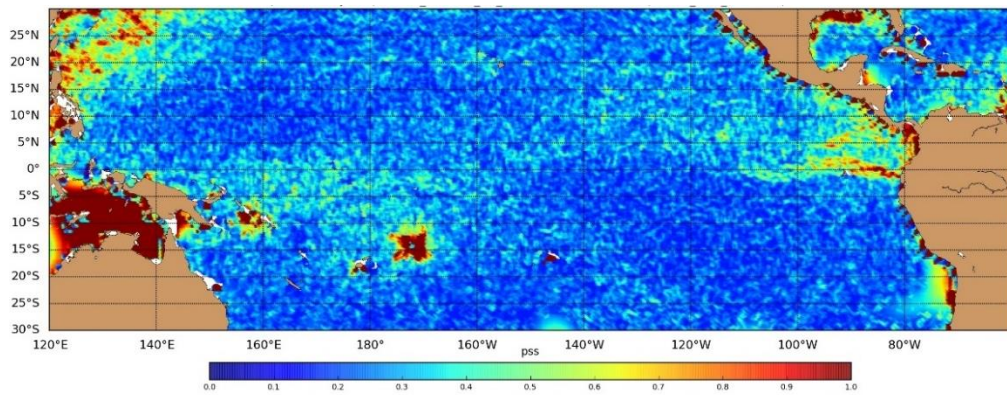


Figure 4: Example of Desroziers ratio ($3^\circ \times 3^\circ$) (see Eq. 3) estimated and applied to the a-priori error (bottom). (week 20-27 January 2016)



5 Figure 5: Example of SSS error (Eq. 4) of SMOS over the Tropical Pacific and used in the data assimilation system for the week 20-27 January 2016.

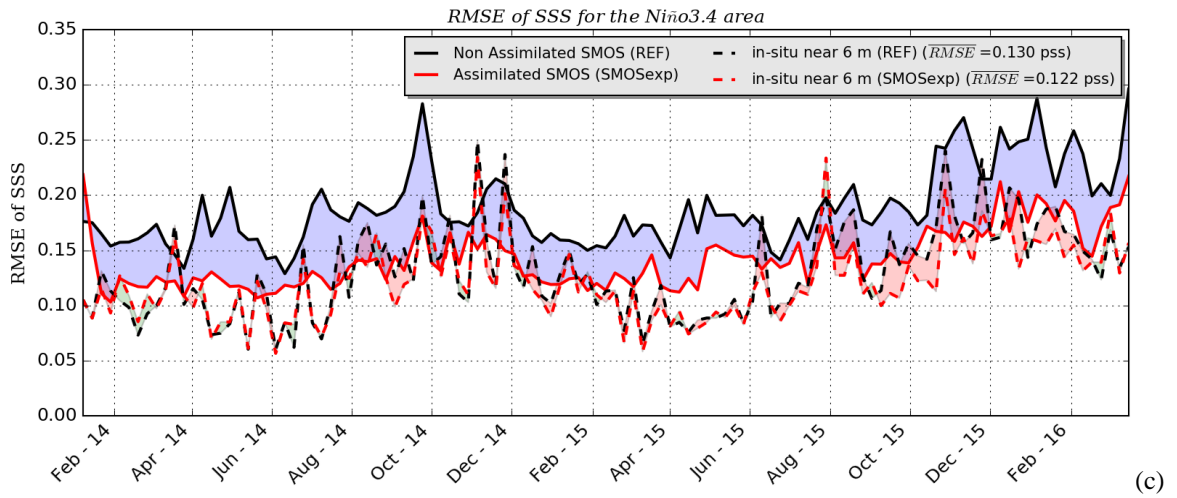
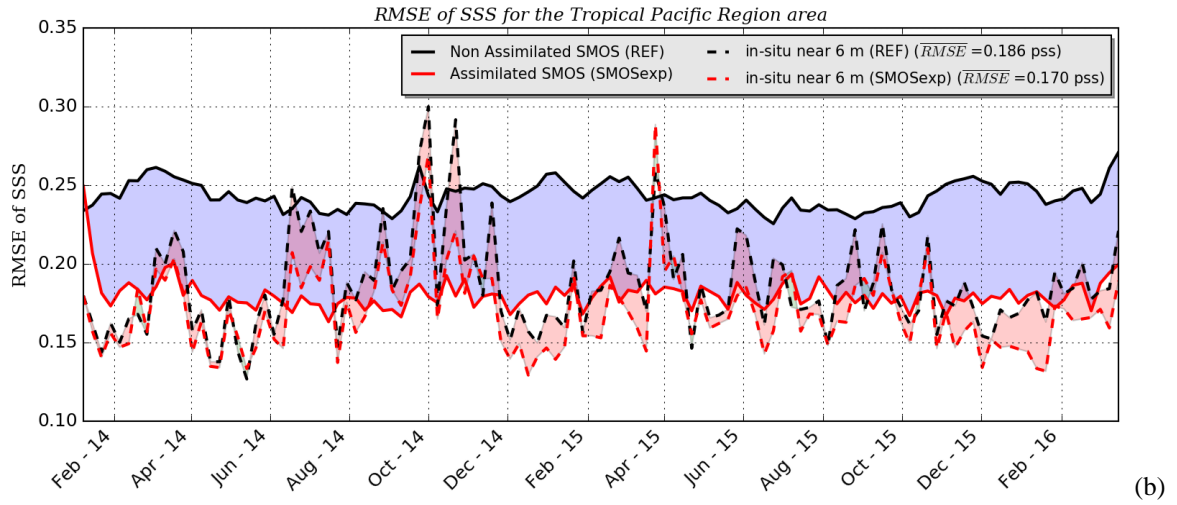
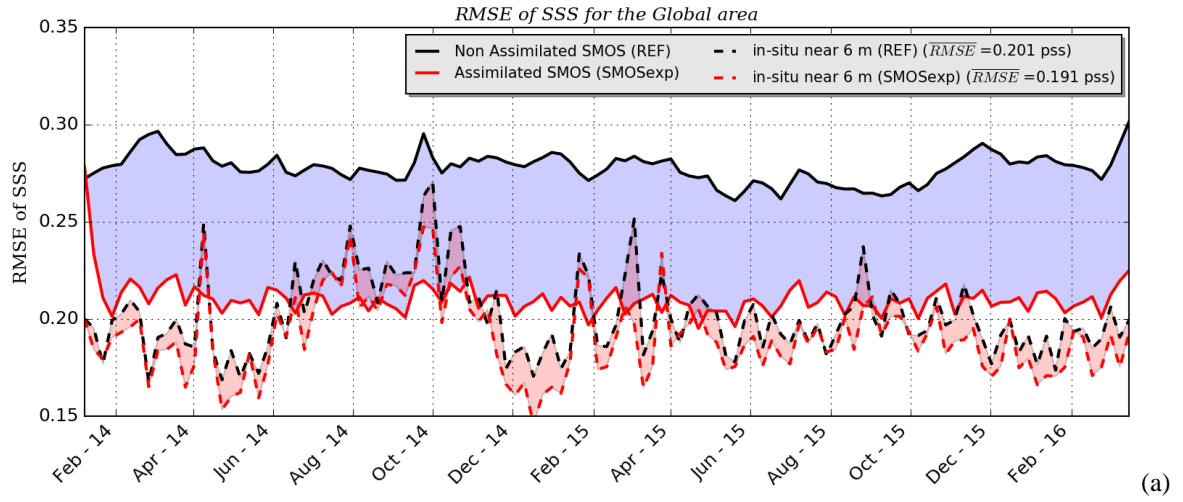


Figure 6: RMSE of SSS with respect to SMOS data (solid lines) and RMSE of salinity near 6 meter depth with respect to in situ salinity data (dashed lines), in the 1-6 day forecast fields in REF (black lines) and SMOSexp (red line) in the global domain (a), the Tropical Pacific (b) and in the Niño3.4 region (c). RMSEs are evaluated for each weak and the mean \overline{RMSE} of the in-situ salinity are denoted in the legend. The regions used here have south-west and north-east corners defined as: Tropical Pacific [30°S, 120°E] to [30°N,70°W]; Niño3.4 [5°S, 170°W] to [5°N, 120°W].

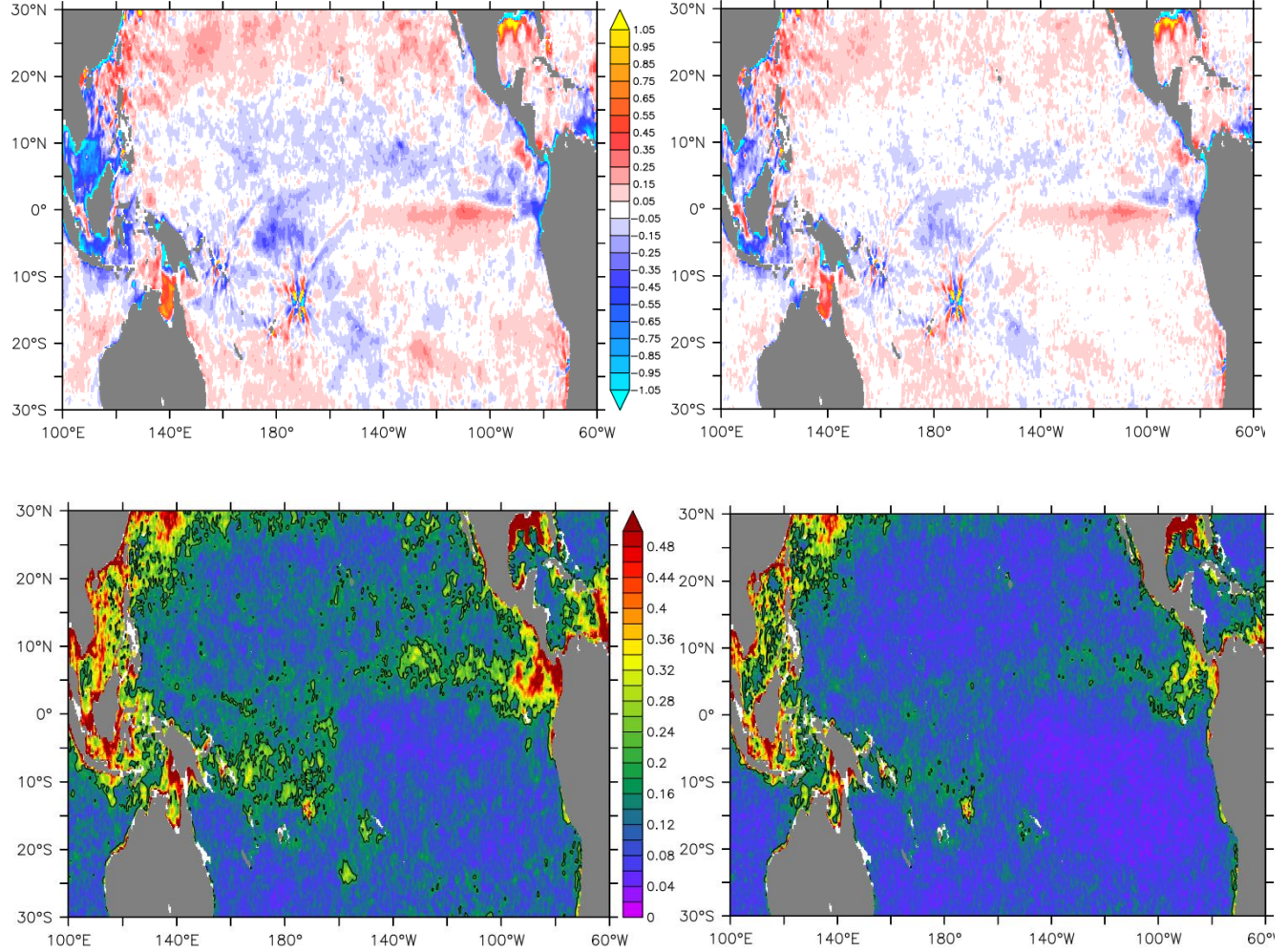


Figure 7: Mean difference (top) and root-mean-square-difference (bottom) of monthly mean SSS with respect to the SMOS data (model minus SMOS) in the analysis fields in REF (left) and SMOSexp (right) experiments on 2015 year.

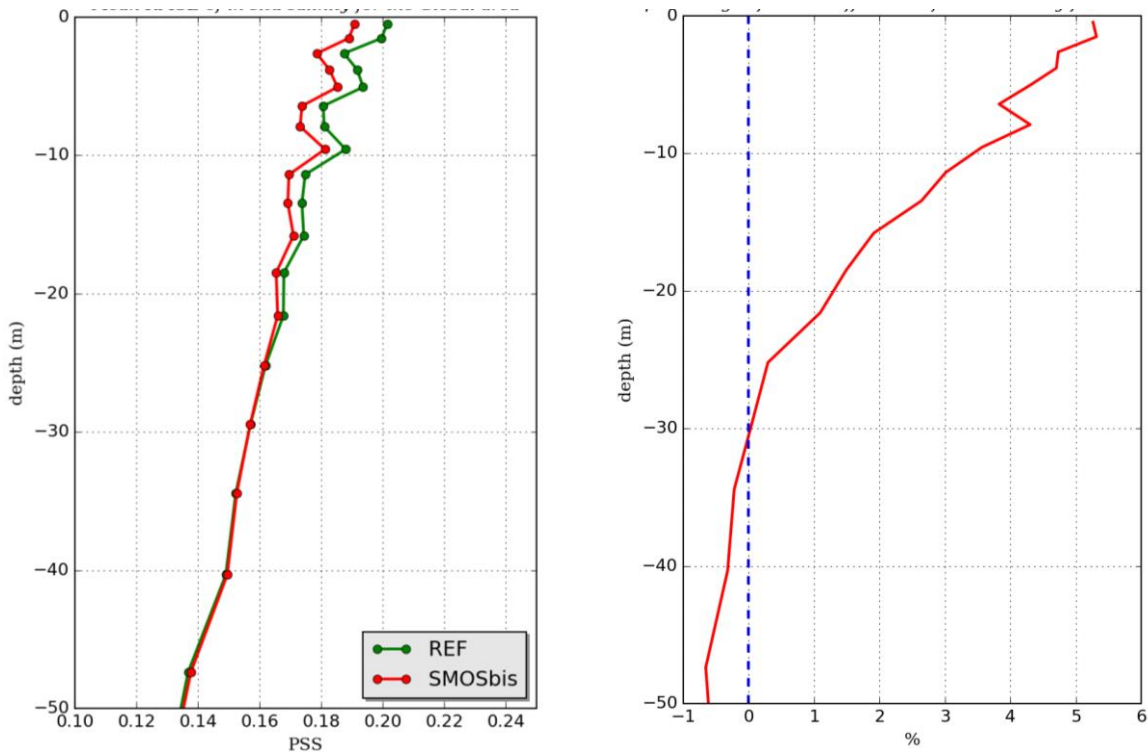


Figure 8: Average salinity RMSE (pss) compared to all in situ measurements (left) over the period 1st Jan 2014 to 2st Mar 2016 in global domain for the *REF* (green line) and *SMOSexp* (red line) experiments as a function of depth over the top 50 m. The corresponding percentage of RMSE difference of all in situ salinity measurements between REF and SMOSexp experiments (right) (positive difference implies a reduction in RMSE by the SSS assimilation).

5

10

15

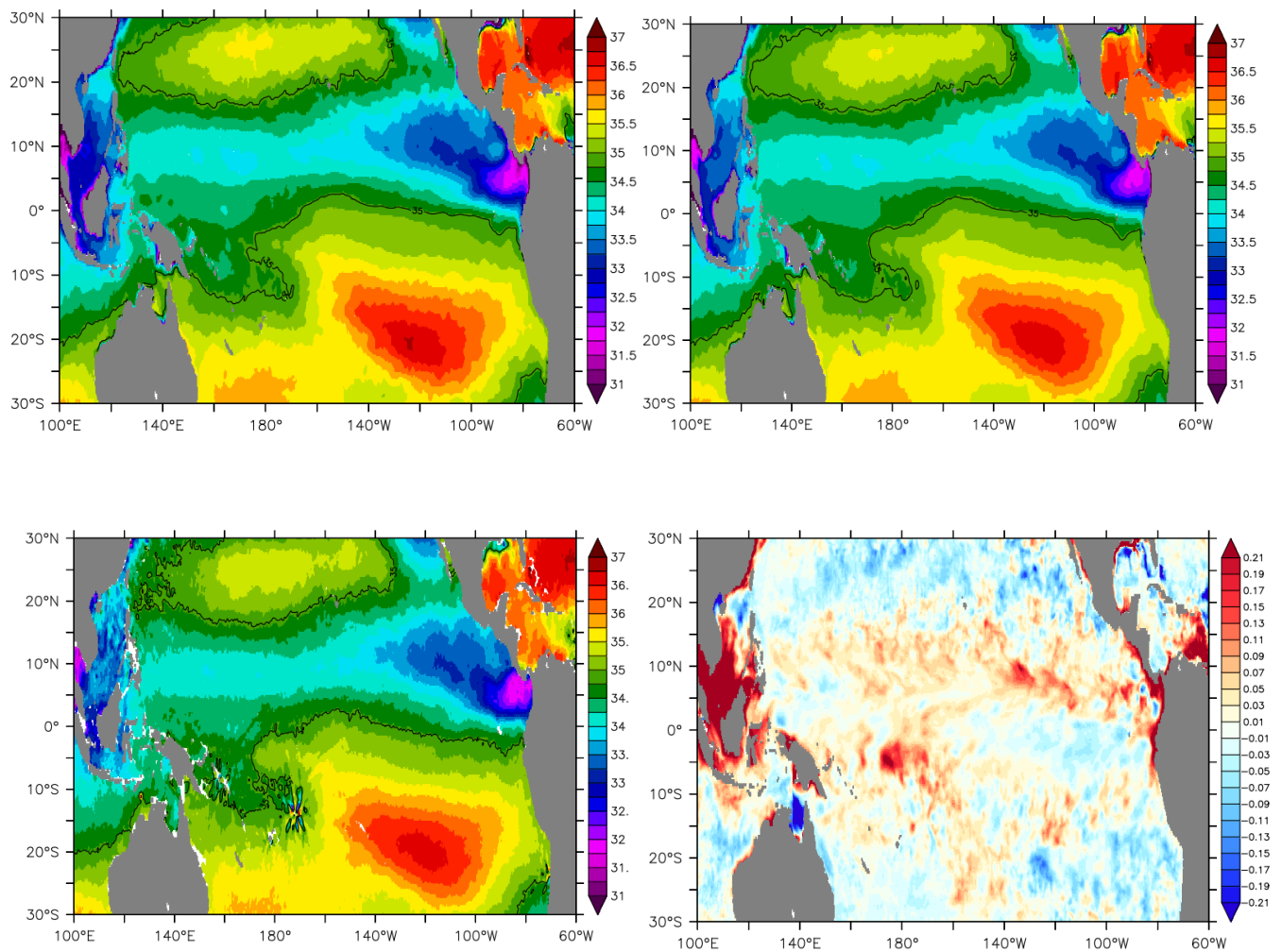


Figure 9: Mean October 2015 SSS estimation from the REF experiment (top, left), the SMOSexp experiment (top, right), the SMOS SSS measurements (left, bottom) and annual mean difference (2015) between the SMOSexp and REF experiment (bottom, right). The isohaline 34.8 pss is the (black solid line) is represented.

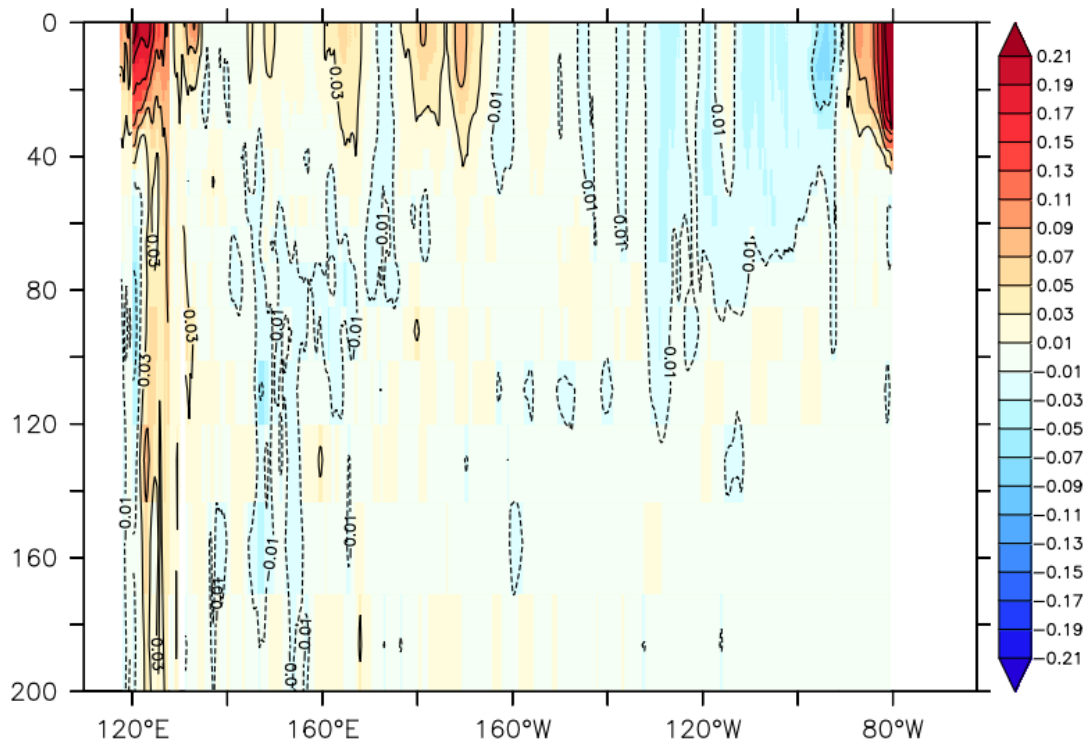


Figure 10: Vertical section along the equator of the mean model salinity difference between the SMOSexp and REF experiments for the year 2015.

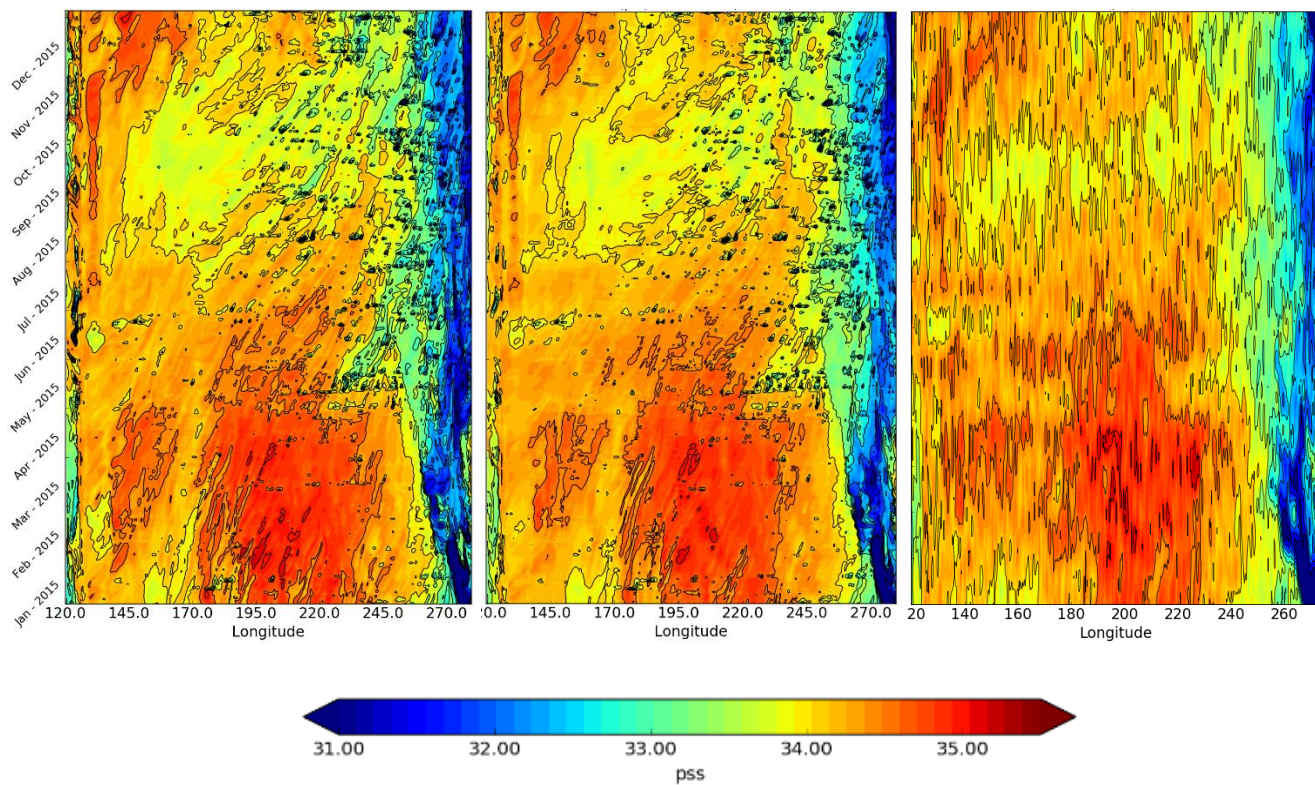


Figure 11: Hovmöller of SSS at 5°N for the REF (left) and SMOSexp (middle) and SMOS data (right)

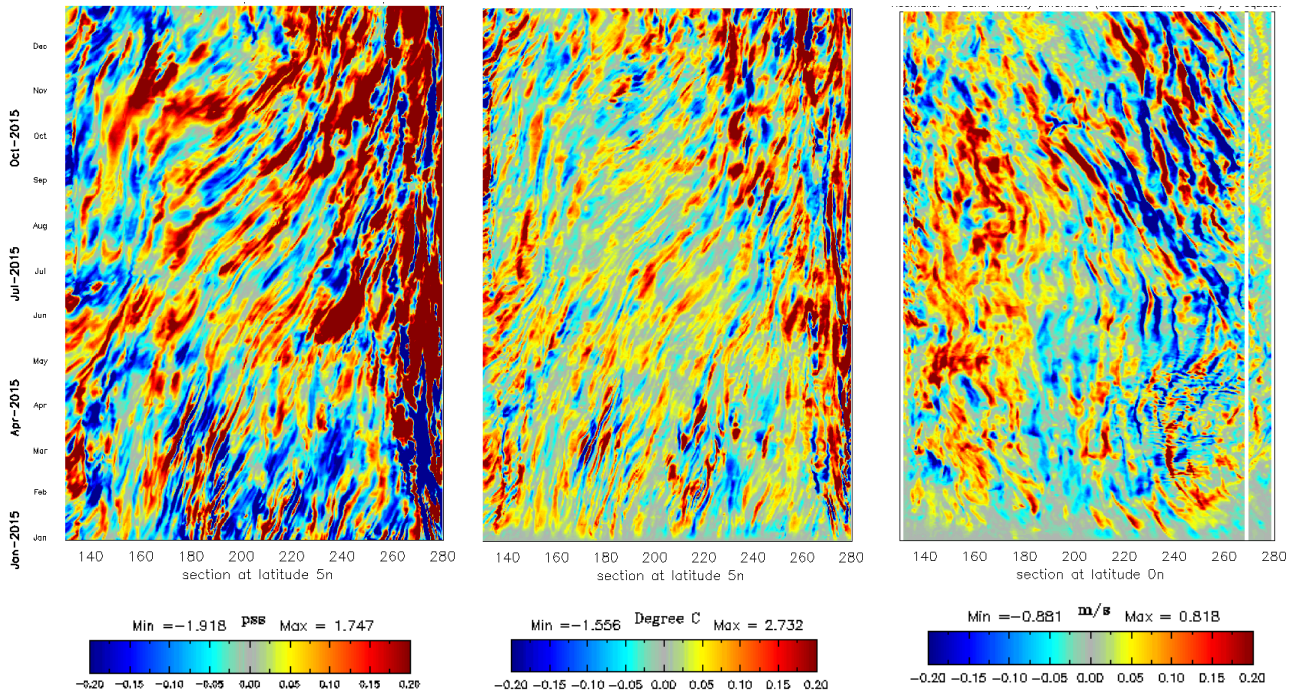


Figure 12: Hovmöller of differences in SSS (left), SST (middle) at 5°N and sea surface zonal velocity (U) (right) at the equator between the SMOSexp and the REF experiment in 2015.

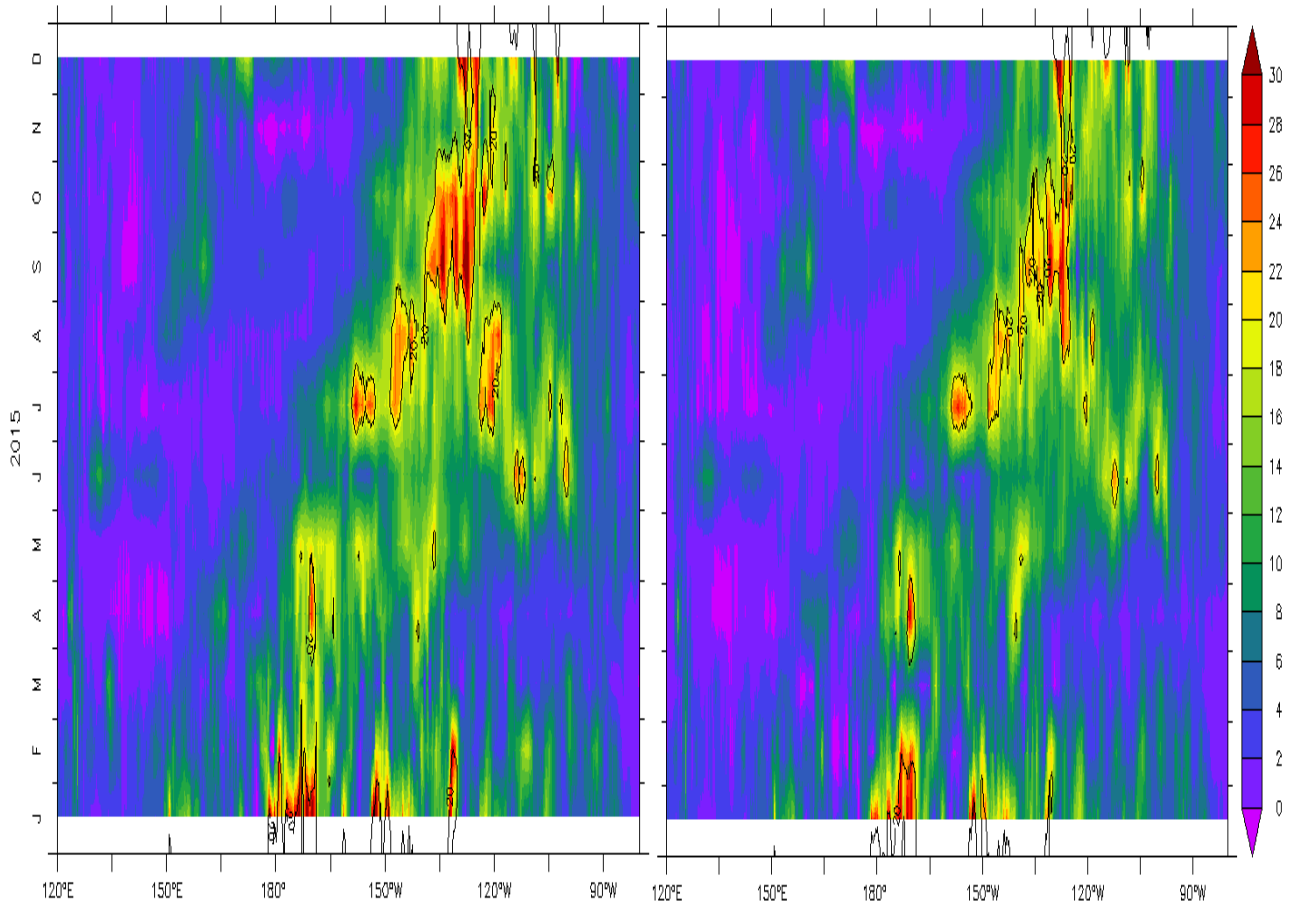


Figure 13: Hovmöller of Barrier Layer Thickness (BLT) at 5°N for the REF experiment in (left) and for the SMOSexp (right) experiment in 2015.

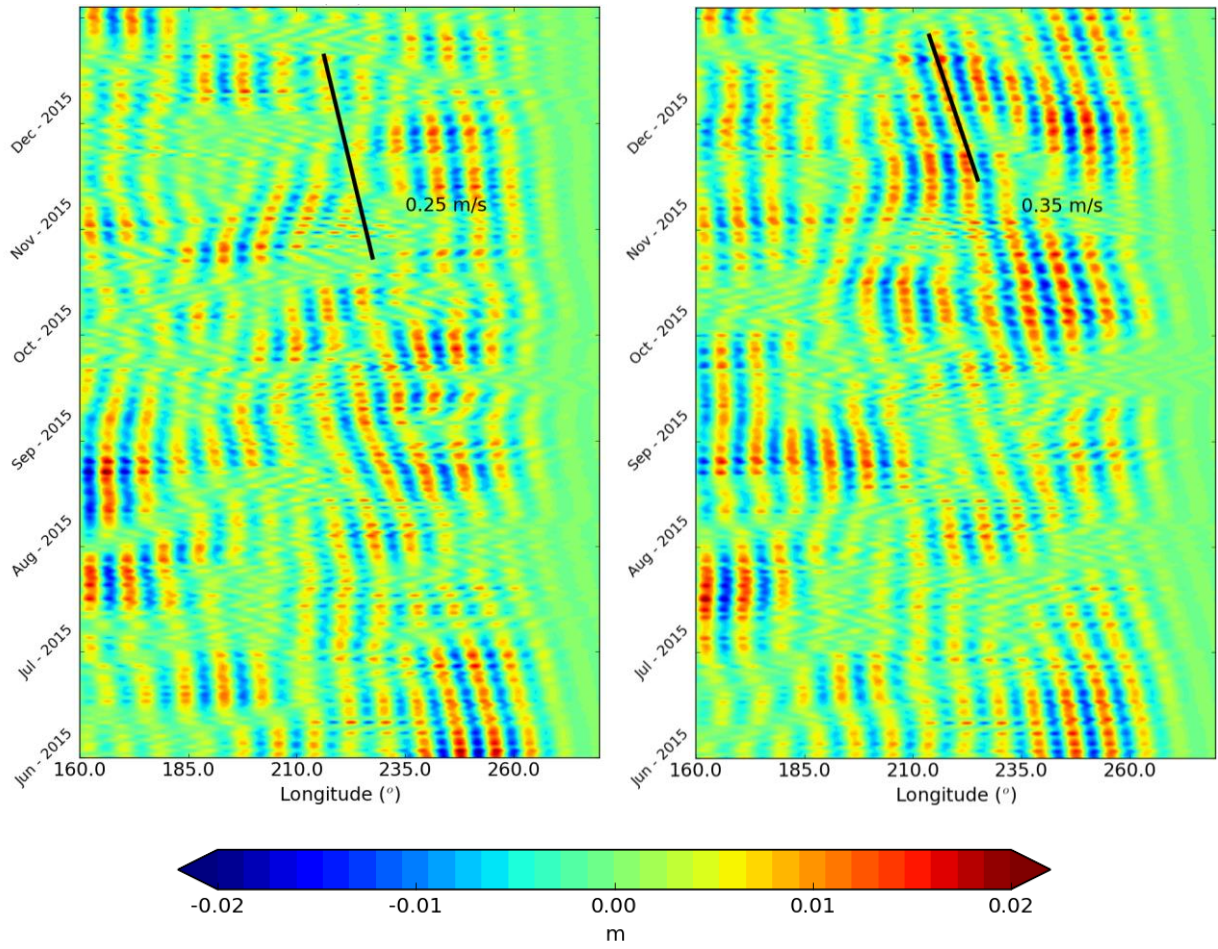
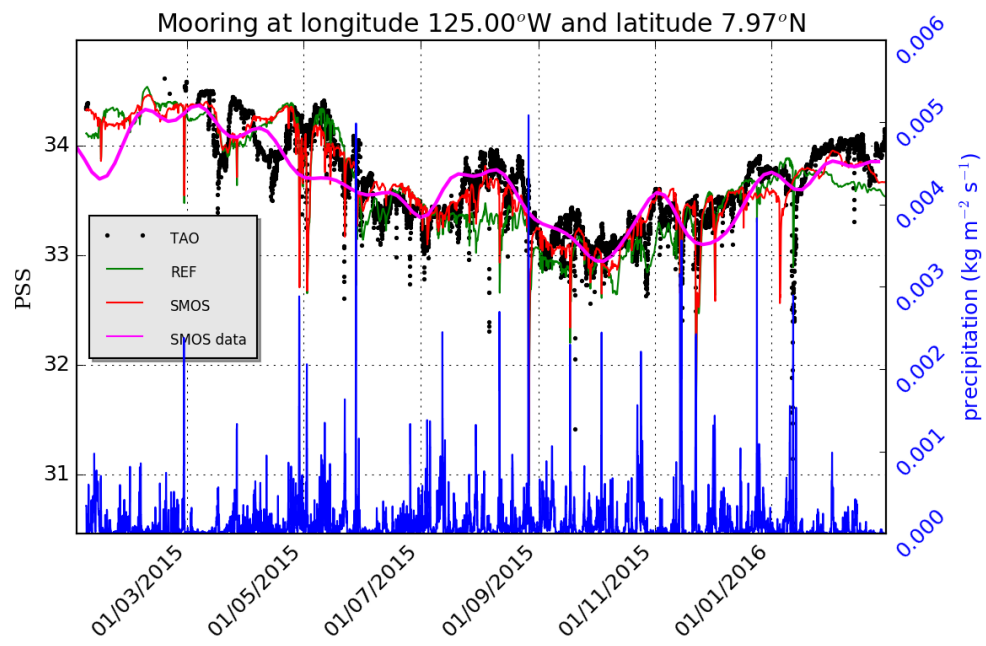
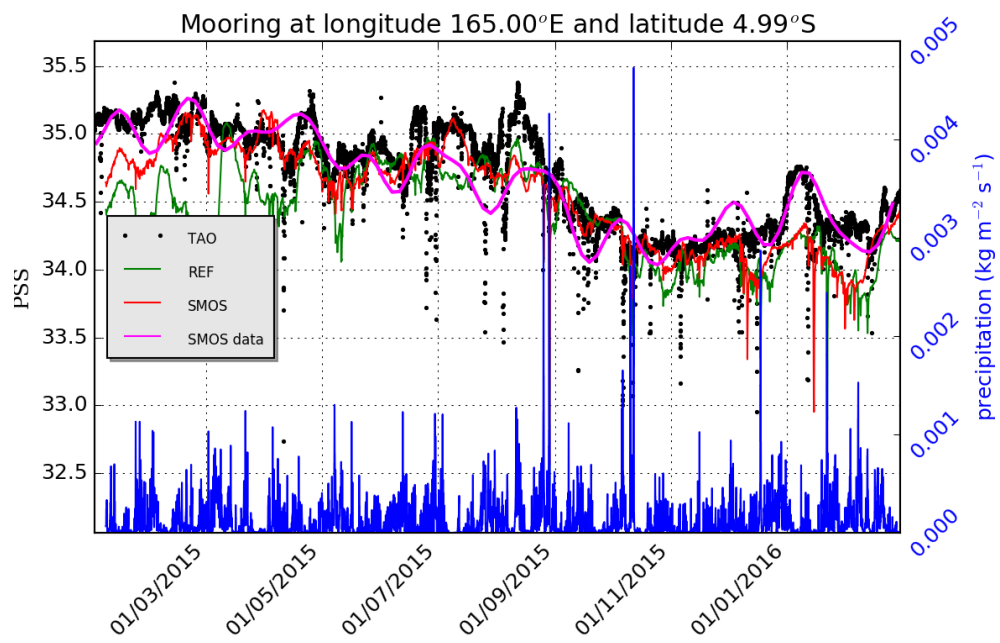


Figure 14: Hovmöller of 28–40 day (33 days) band-passed SSH anomalies at 4°N referenced to the temporal annual mean of June–December 2015 for REF experiment (left) and for SMOSexp experiment (right). The propagation speeds of 0.25 and 0.35 m/s (solid lines) are representative of the propagation speed for the 28–40 day bands.



(a)



(b)

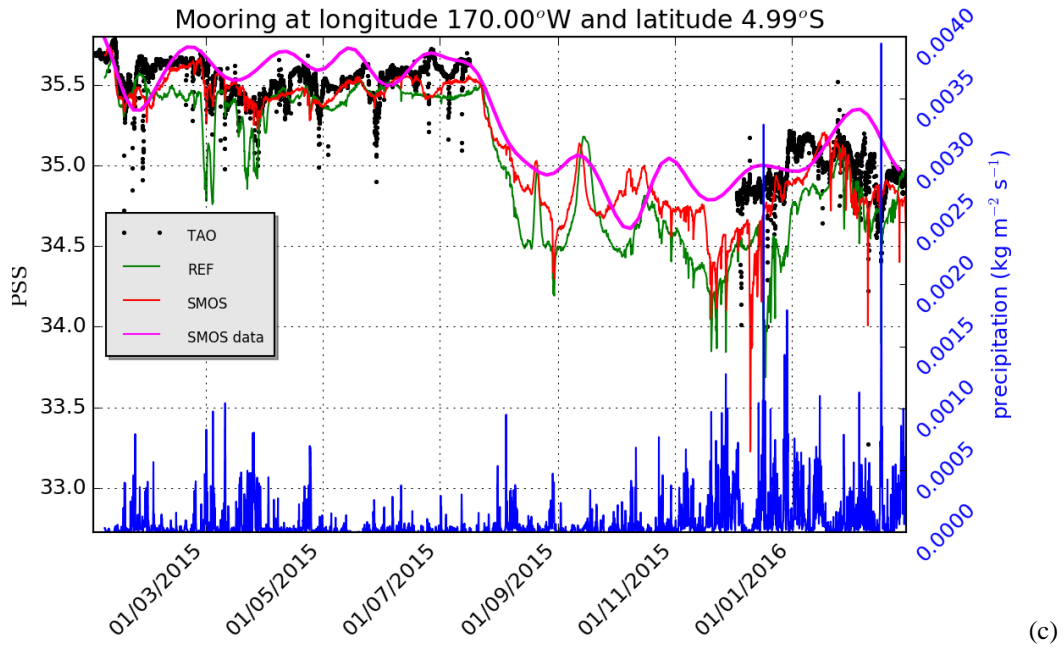


Figure 15: Time evolution of the hourly TAO observed salinity (black), the hourly model REF (green), SMOSexp (red) simulations and the assimilated SMOS data (magenta) at three different TAO moorings locations, cold tongue (a) ($125^{\circ}\text{W}, 7.97^{\circ}\text{N}$), warm pool (b) ($165^{\circ}\text{E}, 4.99^{\circ}\text{S}$) and (c) salt front ($170^{\circ}\text{W}, 4.99^{\circ}\text{S}$) from January 2015 to March 2016. The precipitation rate (blue line) coming from the atmospheric ECMWF forcing is superimposed

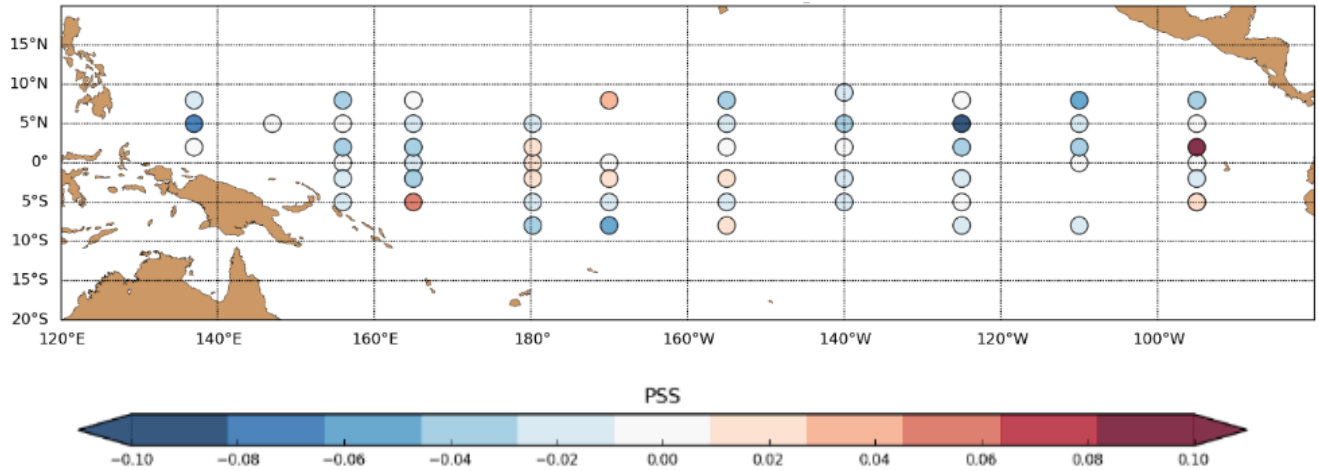


Figure 16. Difference in model salinity RMSD (pss) at 1 m depth calculated against the 1 m depth TAO mooring salinity values (SMOSexp - REF) calculated over the period 1st Jan 2014 to 16th March 2016 (negative/positive difference implies a reduction/increase in RMSD by the SMOS assimilation). Moorings are only included if they have more than 1 week of measurements during the period.

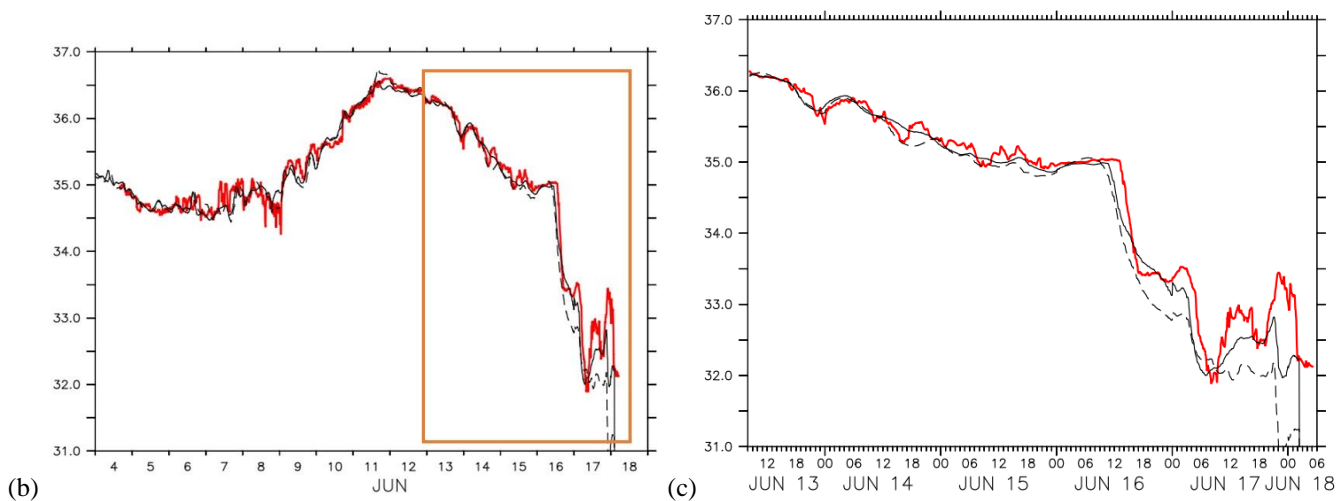
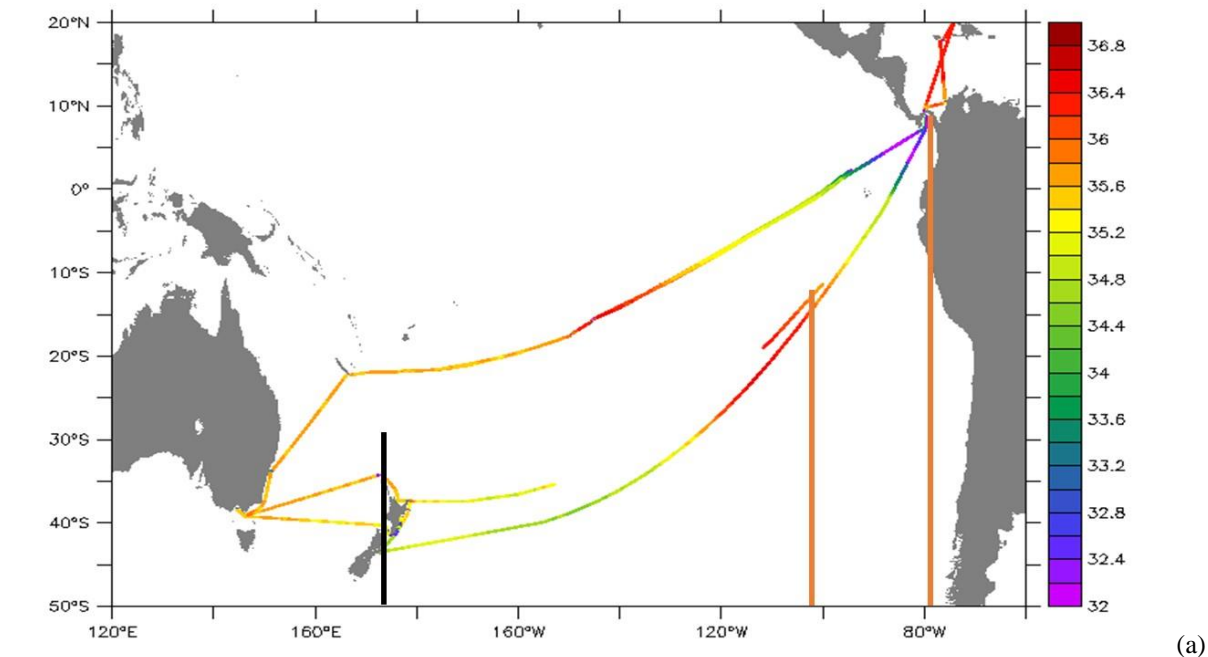


Figure 17: Ship route of the Matisse with TSG salinity observations (PSS) (a) and TSG Salinity observations compared to near sea surface salinity analysis (b,c) from the OSEs (red line= observations, dashed line= REF, black solid line = SMOSexp). A zoom (orange rectangle) is shown on figure (c).

Instrumental errors ($R_{inst.}$)	
Altimetry	
JASON2, ALTIKA/SARAL	2 cm
HAIYANG-2A	4 cm
SST	
OSTIA L4	0.5°C
In-situ at sea surface	
XBT, moorings, Argo floats, sea mammals	0.03°C and 0.0075 pss

Table 1: Instrumental errors used for the current operational system.

Experiment name	Period	Assimilated observations	SSS product
Reference (REF) or control run	Jan 2014- March 2016	Regular observation data without satellite SSS.	No SSS assimilation
SMOSexp	Jan 2014 - March 2016	Regular observation data plus SMOS satellite SSS observations.	4-day 0.25°x0.25° SMOS data from LOCEAN (L3-Debiased-Locean-v2)

Table 2: Experiment descriptions.

Regions [south-west to north-east corners]	Percentage of RMSE difference of SSS when SMOS SSS is assimilated and mean number of observations			
	SMOS SSS		In situ salinity near 6 m depth	
	%	Mean number of obs./week	%	Mean number of obs./week
Global ocean	24 %	372,000	4.7 %	1500
Tropical Pacific [30° S, 120° E] to [30° N, 70° W]	26 %	165,000	7.9 %	500
Niño 3.4 [5°S, 170°W] to [5°N, 120°W]	23 %	9,500	4.8 %	36
Niño 4 [5°S, 160°E] to [5°N, 150°W]	22 %	9,500	6.7 %	38
Niño 3 [5°S, 150°W] to [5°N, 90°W]	25 %	11,400	3.3 %	57
North Tropical Pacific [8°N, 160°E] to [20°N, 100°W]	30 %	22,300	10 %	33
South Tropical Pacific [20°S, 160°E] to [8°S, 90°W]	24 %	24,000	6.6 %	64

Table 3: Percentage of RMSE difference of SSS for SMOS and for in-situ salinity at 6 m depth in different regions. The average number of SSS data assimilated per week is also indicated.